Enterotoxigenic *Escherichia coli* heat-labile toxin drives enteropathic changes in small intestinal epithelia

Alaullah Sheikh[1], Brunda Tumala[1], Tim J. Vickers[1], John C. Martin[2], Bruce A. Rosa[1,2], Subrata Sabui[5,6], Supratim Basu[1], Rita D. Simoes[1], Makedonka Mitreva[1,2], Chad Storer[2,3], Erik Tyksen[2,3], Richard D. Head[2,3], Wandy Beatty[4], Hamid M. Said[5,6], and James M. Fleckenstein[1,7].

Division of Infectious Diseases[1], Department of Medicine, Washington University School of Medicine, St. Louis, MO 63110, USA.

The McDonnell Genome Institute[2], Washington University School of Medicine, St. Louis, MO 63110, USA.

Department of Genetics[3], Washington University School of Medicine, St. Louis, MO 63110, USA.

Department of Molecular Microbiology[4], Washington University School of Medicine, Saint Louis, Missouri, USA 63110.

Departments of Medicine and Physiology/Biophysics, School of Medicine, University of California-Irvine, Irvine, CA[5]; 92697.

Department of Research, VA Medical Center, Long Beach, CA[6]; 90822

Infectious Diseases, Medicine Service, Veterans Affairs Saint Louis Health Care System, Saint Louis Missouri, USA 63106[7].

corresponding author
James M. Fleckenstein
Division of Infectious Diseases
Department of Medicine
Washington University School of Medicine
Campus Box 8051
660 South Euclid Avenue
Saint Louis Missouri, USA 63110
p 314-362-9218fi
jfleckenstein@wustl.edu

abstract

Enterotoxigenic *E. coli* (ETEC), produce heat-labile (LT) and/or heat-stable (ST) enterotoxins, and are a common cause of diarrhea in children of resource-poor regions. ETEC have also been linked repeatedly to poorly understood sequelae including enteropathy, malnutrition, and growth impairment. While the cellular actions of ETEC enterotoxins leading to diarrhea are well-established, their potential contribution to subsequent pathology is unclear. LT stimulates cellular cAMP production to activate protein kinase A (PKA) which phosphorylates cellular ion channels that drive export of salt and water into the intestinal lumen resulting in diarrhea. However, as PKA exhibits broad kinase activity and its activated catalytic subunits modulate transcription of many genes, we interrogated the transcriptional profiles of LT-treated small intestinal epithelia. These studies demonstrated toxin-induced changes in hundreds of genes including those required for biogenesis and function of the brush border, the major site absorption of nutrients, and suppression of a key transcription factors, HNF4 and SMAD4, critical to differentiation of intestinal epithelia. Accordingly, LT treatment of intestinal epithelial cells significantly disrupted the absorptive microvillus architecture and altered transport of essential nutrients. In addition, challenge of neonatal mice with LT-producing ETEC recapitulated the architectural derangement of the brush border while maternal vaccination with LT prevented brush border disruption in ETEC-challenged neonatal mice. Finally, mice repeatedly challenged with toxigenic ETEC exhibited impaired growth recapitulating the multiplicative impact of recurring ETEC infections in children. These findings highlight impacts of ETEC enterotoxins beyond acute diarrheal illness and may inform approaches to mitigate and prevent major sequelae including malnutrition that impact millions of young children.

55

56 ## Introduction

57 Infectious diarrhea remains a leading cause of death and morbidity among young children in low-middle
58 income countries where access to clean water and sanitation remain in short supply[1]. Enterotoxigenic *E. coli*
59 (ETEC), initially discovered as a cause of severe, cholera-like illness[2], are one of the most common pathogens
60 associated with moderate-severe diarrhea among children under the age of five years[3,4], and are perennially the
61 most common cause of diarrhea in travelers[5] to endemic regions where these organisms are thought to account
62 for hundreds of millions of cases of diarrheal illness each year[6].

63 Importantly, ETEC infections have been linked to non-diarrheal sequelae including "environmental enteric
64 dysfunction (EED)," a condition characterized by impaired nutrient absorption, impaired growth[7,8] and
65 malnutrition,[9,10] adding significantly to the morbidity as well as deaths from diarrhea and other infections[11]. The
66 risk of stunting multiplies with each episode of diarrheal illness in children under the age of two years[12], a period
67 during which children residing in impoverished areas commonly sustain multiple ETEC infections[8]. However,
68 the molecular pathogenesis underlying the intestinal changes associated with EED, and the contribution of
69 individual pathogens including ETEC remain poorly understood.

70 Similarly, toxin-producing *E. coli* have also been repeatedly identified in patients with tropical sprue[13-15], a
71 condition classically described in adults residing for extended periods of time in areas where ETEC diarrheal
72 disease is common. Like EED, tropical sprue is associated with changes to the small intestinal villous
73 architecture, including ultrastructural alteration of the epithelial brush border formed by the microvilli[16,17],
74 nutrient malabsorption, and wasting.

75 The basic molecular mechanisms underpinning acute watery diarrhea caused by ETEC are well-
76 established[18]. ETEC produce heat-labile (LT) and/or heat-stable (ST) enterotoxins that activate production of
77 cAMP and cGMP second messengers respectively, leading to activation of cellular kinases that in turn modulate
78 the activity of sodium and chloride channels in apical membrane of intestinal epithelial cells to promote net
79 efflux of salt and water into the intestinal lumen resulting in watery diarrhea.

80 LT and cholera toxin (CT) share ~85 % amino acid identity, and both toxins exert their major effects on the
81 cell through the ADP-ribosylation of the alpha subunit of Gs (Gsα), a stimulatory intracellular guanine
82 nucleotide-binding protein. Inhibition of Gsα GTPase activity leads to constitutive activation of adenylate
83 cyclase and increased production of intracellular cAMP[19].

84 In its central role as a second messenger, cAMP governs a diverse array of cellular processes[20] and
85 modulates transcription of multiple genes through a number of cAMP-responsive transcriptional activators and
86 repressors[21] . cAMP activates protein kinase A (PKA), a heterotetramer, by liberating its two regulatory subunits
87 from the catalytic subunits which are then free to phosphorylate a wide variety of cytoplasmic and nuclear
88 protein substrates[22]. PKA largely regulates transcription by phosphorylation of transcription factors including
89 the cyclic AMP response element binding protein (CREB) and the cAMP-response element modulator (CREM)
90 which bind cAMP response elements (CRE) in the promoter regions of target genes[21-23].

91 Notably, cholera toxin (CT), LT, and dibutyryl-cyclic AMP all induce hypersecretion and impact the
92 architecture of gastrointestinal epithelia in rodent small intestine [24], while small intestinal biopsies of patients
93 with acute cholera exhibit marked changes in the ultrastructure of the intestinal brush border, the major
94 absorptive surface in the small intestine[25,26], including shortening and disruption of the microvilli. Consistent
95 with these observations, studies of young children less than two years of age in Bangladesh have specifically
96 associated LT-producing ETEC with undernutrition[27], suggesting that heat-labile toxin may exert effects on
97 intestinal mucosa that extend beyond acute diarrheal illness.

98 Here we demonstrate that in addition to the canonical effects of LT on cellular export of salt and water into
99 the intestinal lumen, this toxin impacts multiple genes involved in formation of microvilli, resulting in marked
100 alteration of the architecture of the intestinal brush border, the major site of nutrient absorption in the small
101 intestine. These effects are compounded by alteration of solute transporters within the brush border epithelia,
102 potentially disrupting the absorption of multiple essential nutrients.

103 ## Results

104 ### Heat-labile toxin markedly alters the transcriptomes of intestinal epithelial cells.

105 Commensurate with the importance of cAMP as a second messenger, we found that compared to either
106 untreated controls or cells treated with a catalytically inactive (E211K) mutant of LT, wild type LT holotoxin
107 substantially modulated transcription of many genes in intestinal epithelial cells. In RNAseq studies of polarized
108 Caco-2 intestinal epithelial cells we found that 3,832 genes were significantly ($p \leq 10^{-5}$) upregulated and 3687
109 downregulated in response to LT, while the inactive toxin failed to induce significant changes in the
110 transcriptome (figure 1a). However, Caco-2 cells are derived from distant metastases of a colon cancer tumor in
111 which transcriptomes would likely be altered relative to untransformed intestinal epithelia[28,29], and cAMP
112 signaling is known to be aberrant in some transformed cells[23]. Therefore, to examine a more physiologically
113 relevant target, we next examined the impact of LT on differentiated small intestinal enteroids. Here, we found
114 that far fewer genes were differentially expressed ($\leq 10^{-5}$) with 746 significantly upregulated, and 561
115 downregulated in response to intoxication with LT (figure 1b). Notably, however we found substantial
116 statistically significant overlap in genes significantly modulated in Caco-2 cells and enteroids (supplemental
117 table 3, supplemental dataset 1) with the transcription of hundreds of genes significantly up- or down-regulated
118 in both groups. Gene ontology enrichment analysis as well as ontology-independent investigation of genes
119 (CompBio, supplemental figure 1) modulated by the toxin highlighted multiple cellular components associated
120 with both the development and function of the absorptive surface of the small intestine (supplemental dataset
121 2).
122

123 ### Heat-labile toxin impairs development of small intestinal microvilli.

124 Small intestinal enterocytes are each covered with hundreds of microvilli, complex structures comprised of a
125 central core of actin filaments within protrusions of the plasma membrane. Collectively, the luminal surface of
126 the intestine formed by these microvilli, known as the brush border, represents the major absorptive surface of

127 the gastrointestinal tract. Three major classes of proteins are required for the biogenesis of microvilli[30] (figure
128 2a). These include (1) proteins such as villin, epsin, plastin, and EPS8 that bundle parallel clusters of actin
129 filaments; BAIP2L1 (IRTKS) responsible for recruiting the EPS bundling protein to the tips of microvilli[31]; (2)
130 ezrin, myo1a[32], myo6 that link the actin cytoskeleton with the plasma membrane; and (3) protocadherin
131 molecules CDHR2 and CDHR5 engaged in extracellular heterotypic complexes between the tips of the
132 microvilli[30] that are stabilized by a tripartite complex of MYO7B, ANKS4B[33], and USH1C[33]. Interrogation of
133 transcriptional profiles indicated that the transcription of each of these classes of genes was significantly
134 altered following exposure to wild type heat-labile toxin (figure 2b). Similarly, RT-PCR confirmed decreased
135 expression of multiple genes involved in microvilli biogenesis, including VIL1 encoding villin (figure 3a), and we
136 were able to demonstrate that production of villin was depressed in polarized small intestinal enteroids (figure
137 3b supplemental figure 2). In addition, TEM images of polarized small intestinal enteroids exposed to heat-
138 labile toxin demonstrated significantly shortened and disorganized microvillus structures on the apical surface
139 of enterocytes (figure 3c).

140 **Heat-labile toxin modulates the transcription of multiple brush border nutrient transport genes.**

141 The human solute carrier (SLC) gene superfamily is comprised of more than 50 gene families thought to
142 encode more than 300 functional transporters[34]. Many of the SLC proteins are enriched in the small intestinal
143 brush border where they transport critical nutrients including amino acids, oligopeptides, sugars, and vitamins.
144 We found that transcription of many SLC genes was altered in Caco-2 cells as well as small intestinal enteroids
145 (figure 4a). These included transporters for Zinc, known both to be deficient in children with enteropathy[35], and
146 a micronutrient critical for intestinal homeostasis. Likewise transcription of SLC19A3 encoding the principal
147 SLC responsible for uptake of the water-soluble B vitamin thiamine (vitamin B1)[36] by differentiated intestinal
148 epithelial cells lining the surface of intestinal villi of the proximal small intestine[37,38](figure 4b) was repressed as
149 was production of the corresponding protein (supplemental figure 3a). Moreover, we found that LT treatment
150 of human small intestinal organoids also interfered with transcription of the cis regulatory element specificity

151 protein 1 (SP-1) previously shown to govern the transcription of SLC19A3[39-41] (figure 4c, supplemental figure
152 3b). Finally, we found that thiamine transport was significantly depressed following exposure to LT (figure 4d)
153 providing additional evidence that ETEC can impair transport of critical nutrients.

154 **LT-producing ETEC disrupt the absorptive architecture of the small intestine**

155 To further study the potential impact of ETEC toxins on the intestinal architecture, we performed challenge
156 studies in infant mice. Compared to sham-challenged (PBS) controls, or mice challenged with a toxin deficient
157 strain of ETEC, we again noted down-regulation of genes involved in F-actin bundling, membrane cross-linking,
158 and intermicrovillus adhesion complex formation, all required for intestinal microvilli (figure 5a) biogenesis.
159 Likewise, on examination of small intestinal villi we found that production of villin in enterocyte brush borders
160 was substantially decreased relative to sham challenged controls (figure 5b,c). In mice challenged with a wild
161 type ETEC isolate that makes ST and LT, but not a LT/ST-toxin-negative mutant (jf4763, supplemental table 1),
162 we observed significant alteration in architecture of the intestinal brush border with significant shortening and
163 disorganization of the microvilli (figure 5d,e; supplemental figure 4a-d) reminiscent of the earlier ultrastructural
164 studies of patients with tropical sprue [17] and *V. cholerae* infections[25]. Similarly, we found that in mice challenged
165 with a strain containing an isogenic mutation in *eltA* (jf571, supplemental table 1) encoding the LT A subunit,
166 which still makes heat-stable toxins, the microvillus architecture was preserved (figure 5f,g), suggesting that LT
167 is the principal toxin underlying the enteropathic changes to the enterocyte surfaces.

168 Despite the dramatic toxin-dependent changes to the absorptive surface of the intestine, the early growth
169 kinetics of suckling mice challenged a single time with either wild type bacteria or a heat-labile toxin deletion
170 mutant were surprisingly similar (supplemental figure 5A) and paralleled those of sham-challenged controls.
171 However, enteropathy in young children is thought to reflect damage elicited by repeated infections. Children
172 in endemic regions typically suffer *multiple* ETEC infections before their 2nd birthday, and the risk of
173 enteropathic sequelae increases multiplicatively per episode[8,42]. Therefore, to assess the contribution of
174 repeated ETEC infections to growth impairment, we compared the growth kinetics of suckling mice challenged

175 a single time to those repeatedly infected with wild type toxigenic ETEC. These studies demonstrated a clear
176 impact of repeated infection on growth (supplemental figure 5B). Finally, we found that the growth kinetics of
177 mice repeatedly challenged with wild type ETEC H10407 was significantly retarded relative to those challenged
178 with the isogenic LT-mutant jf876 (supplemental figure 5C). Therefore, repeated infections in this model appear
179 to recapitulate impacts observed following repeated ETEC infection in children, and our data suggest that these
180 features are at least in part driven by LT.

181 **Maternal vaccination with LT prevents brush border disruption**

182 To address whether enteropathic changes to the small intestine can be prevented by vaccination, and to
183 further define the role of LT, we vaccinated mouse dams with heat-labile toxin and examined the brush border
184 ultrastructure in suckling mice. Vaccinated dams but not sham vaccinated controls expressed significant levels
185 of IgA and IgG in breast milk (figure 6a), consistent with increased levels of antibodies in the stomachs of infant
186 mice (figure 6b). Notably, we found that maternal vaccination with LT completely abrogated changes to the
187 microvilli (figure 6c,d) further substantiating the importance of LT in driving changes to the epithelial
188 architecture.

189 **LT modulates key transcription factors that govern enterocyte development**

190 Despite the marked alteration in transcription mediated by LT the majority of genes critical for brush border
191 development lacked conserved CRE sites [23]. Therefore, we performed transcription factor target enrichment
192 analysis[43,44] to identify potential transcription factors responsible for differential regulation of genes
193 significantly ($P < 0.05$) upregulated or downregulated by LT in both Caco-2 and enteroid RNA-seq datasets
194 (supplemental table 4, supplemental dataset 1). The upregulated genes were most significantly ($p = 4.2 \times 10^{-3}$)
195 linked to transcription factor targets of AP-1 encoded by the *c-jun* gene, previously shown to be regulated by
196 cAMP[45], and to be involved in intestinal epithelial repair[46]. Notably however, downregulated genes were most
197 significantly enriched in targets for the HNF4α transcription factor or its intestine specific paralog HNF4γ ($P =$
198 1.9×10^{-4}) that were recently shown to regulate multiple genes required for brush border development[47,48].

199 Importantly, PKA has also been shown to phosphorylate HNF4 α at a consensus recognition site within the
200 DNA binding domain, shared with HNF4 γ, inhibiting transcription[49].
201 Of note, the transcription of both paralogs was found to be significantly depressed following exposure of
202 intestinal epithelia to LT (figure 7A,B), as were levels of HNF4γ in nuclear fractions from toxin-treated cells
203 (figure 7C), suggesting that activation of cAMP can interfere with transcription mediated by HNF4. To further
204 examine the impact of LT on HNF4-mediated transcription we introduced a transcriptional reporter plasmid
205 containing 6 tandem copies of the HNF4 transcriptional response element (5′- CAAAGGTCA-3′) linked to a
206 human codon optimized *Gaussia princeps* luciferase into Caco-2 cells. These assays demonstrated that HNF4-
207 mediated transcription was dramatically reduced in cells treated with LT (figure 7D). Similarly, we found that
208 relative to nuclei of intestinal epithelia cells in ileal segments from sham-challenged control mice, those from
209 ETEC-challenged mice exhibited significantly less HNFγ (figure 7E) further supporting a role for ETEC in
210 modulating the production of this important transcription factor. Chen, *et al* described a "feed-forward
211 regulatory module" essential to enterocyte differentiation in which HNF4 and SMAD4 transcription factors
212 reciprocally activate each other's transcription. As would be predicted from this model, we found that
213 transcription of SMAD4 was also impaired by LT (supplemental figure 6A,B) leading us to speculate that LT
214 mediated phosphorylation of HNF4 by PKA, interrupts this critical transcription module (supplemental figure
215 6C-E).
216 Collectively, the current studies demonstrate that in addition to their known canonical effects on ion
217 transport that culminate in watery diarrhea, ETEC toxins can drive appreciable derangement of enterocyte
218 architecture and function by interfering with key pathways in intestinal epithelia that govern the formation of
219 mature enterocytes capable of effective nutrient absorption. These findings have important implications for our
220 understanding and prevention of enteropathic conditions linked to ETEC.
221

222 ## Discussion

223 Understanding the molecular events that lead to sequelae of undernutrition and growth faltering following
224 ETEC infections may be key to the effective design of prevention strategies including vaccines[50]. Although the
225 molecular mechanisms involved in the fluid and ion fluxes into the intestinal lumen leading to diarrhea are
226 firmly established, only recently has evidence emerged to suggest that ETEC toxins may incite previously
227 unappreciated changes in small intestinal epithelia[51,52]. The present studies, initiated to identify additional
228 effects of LT, were prompted by an appreciation that cyclic nucleotides, particularly cAMP, govern a multitude
229 of cellular pathways potentially resulting in collateral impacts that extend beyond the acute episodes of
230 diarrhea. Consistent with this model, we found that exposure of intestinal cells to heat-labile toxin altered the
231 transcription of hundreds of genes. A central theme highlighted in the analysis of these transcriptional
232 alterations is that LT affects major classes of genes involved in biogenesis of microvilli and function of the
233 intestinal brush border, the major site of nutrient uptake in the small intestine, potentially offering a direct
234 molecular link to sequelae of malnutrition and impaired growth in children.

235 The potential clinical relevance of the observations reported here is highlighted by remarkably similar
236 ultrastructural alteration of intestinal epithelial cells seen in small intestinal biopsies of patients with acute
237 cholera[25] and tropical sprue[17]. In both entities, the brush border was noted to be abnormal, with shortened,
238 irregular microvilli. Importantly, however despite the structural and functional similarity between LT and CT,
239 clinical cholera, unlike ETEC infections, has not been linked to enteropathy or attendant sequelae. Whether this
240 relates to the repetitive nature of ETEC infections compared to the durable protective immunity that follows a
241 single *V. cholerae* infection[53] is not presently clear. Similarly, while tropical sprue remains a leading cause of
242 malabsorption in regions where infectious diarrhea is prevalent[54-56], the most debilitating forms of this illness
243 have not typically followed isolated cases of traveler's diarrhea, but occur in resident populations or
244 expatriates[57] repeatedly assailed by diarrhea while residing in endemic regions[58]. Likewise, our data also
245 highlight the potential importance of repeated infections on the development of sequelae.

246 The negative impacts of LT on brush border architecture with commensurate reduction in surface area
247 available for nutrient absorption, are compounded by the alteration of multiple SLC genes that encode
248 transporters critical for uptake of essential vitamins and other molecules. Importantly, small intestinal biopsies
249 obtained from Zambian children with enteropathy and refractory stunting exhibited similar changes in SLC
250 gene expression profiles[59]. The decreased transcription of molecules required for intestinal zinc uptake, in cells
251 treated with LT is particularly intriguing given the known aberrations in zinc absorption in children with
252 enteropathy[35,60,61], the possible contribution of zinc deficiency to enteropathic changes[62], and the salutary
253 effects of zinc in treatment of children with diarrhea[63,64].

254 Further study will be needed to precisely delineate the role of ETEC LT and ST enterotoxins, alone and in
255 combination, in driving enteropathic changes to the intestine and sequelae. ST-producing ETEC were most
256 strongly associated with moderate to severe diarrhea in GEMS[3], and follow-on studies of children enrolled in
257 these studies have also linked infections with ETEC encoding heat-stable toxin to growth faltering[7]. However,
258 our earlier analysis of a global collection of more than 1100 ETEC isolates, including those collected in GEMS,
259 demonstrated that slightly more than half of all ST-encoding strains also encoded LT, and that roughly one
260 third of the isolates overall encoded LT alone, ST-LT, or ST only[65]. While LT-producing ETEC have been
261 specifically linked to malnutrition among children in Bangladesh[27], and our *in vitro* and animal studies point to
262 the potential importance of LT, additional effort will be needed to correlate toxin-induced morphologic and
263 functional perturbation of the intestinal brush border with outcomes in children. Importantly, the long-term
264 morbidity associated with ETEC infections does not appear to correlate with the severity of diarrhea as both
265 mild illness[4], and perhaps asymptomatic colonization may lead to growth faltering.

266 Further refinement of animal models that can faithfully recapitulate features of enteropathy are also needed.
267 Indeed, conventional mice lack genes that could be required to reproduce the full effects of ETEC. For instance,
268 each of the carcinoembryonic antigen cell adhesion molecules (CEACAMs) that are substantially upregulated

269 on human small intestinal epithelia in response to LT, and which we have recently shown to play a critical role in
270 ETEC interactions with human small intestine[51], are absent in mice.

271 While the precise mechanism underlying LT-mediated modulation of genes required for microvillus
272 biogenesis and absorptive function of the brush border is presently unclear, stimulation of adenylate cyclase
273 invokes many cAMP-responsive nuclear factors that may serve either to activate or repress transcription. Genes
274 implicated in development of microvilli are mostly devoid of consensus palindromic (TGACGTCA) or "half"
275 (CGTCA) cAMP response element (CRE) sites within their promoter regions for direct modulation by CREB[66],
276 which typically is involved as a transcriptional activator, and both CREB and CREM can yield several
277 alternatively spliced variants that may act as either activators or repressors[67]. cAMP second messaging also
278 engages multiple signaling pathways converging at CREB[68], and PKA can phosphorylate and modulate the
279 activity of multiple transcription factors to act either as transcriptional activators or repressors, including SP1[69].
280 Notably, putative binding sites for HNF4, a cAMP-modulated transcription factor[49] known to regulate genes
281 needed for formation of microvilli[47,48], were significantly enriched in the promotors of genes downregulated by
282 LT. Both HNF4α and HNF4γ possess canonical PKA recognition sites within their DNA binding motifs, and PKA
283 phosphorylation of these sites interrupts transcription[70]. HNF4 activates the transcription of SMAD4, and in
284 turn SMAD4 activates transcription of HNF4[71]. Both transcription factors then engage genes needed for
285 effective differentiation of stem cells to mature enterocytes[71]. Modulation of the activity of this transcription
286 factor by LT would therefore be predicted to have a marked impact on pathways critical to intestinal epithelial
287 homeostasis.

288 We should also note that increases in cellular cAMP can impact multiple cellular pathways independent of
289 PKA. Included among these are pathways governed by a more recently discovered family of cellular cAMP-
290 binding molecules, exchange proteins activated by cAMP (EPACs). EPACs appear to play critical roles as
291 guanine exchange factors that regulate GTPase proteins[72] and are in involved in complex signaling networks
292 implicated in cell growth, differentiation, and morphogenesis[73,74].

293 cAMP can also exert potent epigenetic influences on transcription. CREB-binding protein (CBP) possesses
294 intrinsic histone acetyl-transferase (HAT) activity[75], and can therefore modulate chromatin remodeling,
295 enhancing access of transcription factors. In addition, cAMP messaging through PKA leads to phosphorylation-
296 dependent activation of the histone demethylase enzyme PHF2 to promote the transcription of multiple genes
297 that can impact transition from stem cells to epithelial cells[76].

298 Altogether it seems likely that multiple pathways governed by increases in cellular cAMP may underlie the
299 morphologic and functional disruption of the brush border epithelial observed in our studies. Nevertheless, the
300 data presented here provide compelling evidence that the heat-labile toxin of ETEC ultimately impacts multiple
301 genes required for the biogenesis and function of the brush border, the major site of nutrient absorption in the
302 human small intestine. The findings may have significant implications for our understanding of sequelae linked
303 to ETEC including environmental enteropathy in young children, and tropical sprue in adults. The increased
304 acknowledgement of long-term morbidity linked to ETEC and an improved understanding of the role of ETEC
305 enterotoxins as drivers of this morbidity may also strengthen the case for vaccines[50] specifically engineered to
306 prevent both the acute illness and sequelae.

307

308 ## Methods

309 ### Culture and differentiation of Enteroids

310 Biopsy samples from adult patients undergoing routine endoscopy were obtained at Washington University
311 School of Medicine after patient consent and approval from the Institutional review board.

312 Purified crypt cells from the ileum were re-suspended in Matrigel (BD Bisosciences, San Jose, California,
313 USA) and 15 µL of re-suspended matrix gel was added to each well in 24 well plates. Plates were incubated at
314 37° C and 5% CO2 with 50% L-WRN conditioned media (CM) and 50% primary culture medium (Advanced
315 DMEM/F12, Invitrogen) supplemented with 20% FBS, 2 mM L-glutamine, 100 units/mL penicillin, 0.1 mg/mL
316 streptomycin, 10 µM Y-27632 (ROCK inhibitor, Tocris Bioscience, R&D systems, Minneapolis, MN, USA), and 10
317 µM SB431541 (TGFBR1 inhibitor, Tocris Bioscience, R&D systems).

318 To induce differentiation and polarization of enteroids, cells were washed once to remove Matrigel, followed
319 by trypsinization and centrifugation at 1100 x g for 5 minutes. Cells were then re-suspended in 1:1 CM and
320 primary medium with Y-27632 and SB431541 as described above. Cells were then plated on semiporous filters
321 (Transwells®, 6.5 mm insert, 24 well plate, 0.4 µm polyester membrane, Corning Incorporated, Kennebunk,
322 ME, USA) that had been previously coated with Collagen IV (Millipore Sigma). Transwell® inserts were rinsed
323 with DMEM/F12 with Hepes, 10% FBS, L-glutamine, Penicillin, and streptomycin. Cells were allowed to grow to
324 confluency in 50% conditioned media (CM) and then changed to differentiation medium (5% CM in primary
325 medium + ROCK inhibitor) for 48 hours. Differentiated cells were used for toxin treatment.

326 ### Propagation of Caco-2 cells

327 Caco-2 intestinal epithelial cells were obtained from ATCC (ATCC HTB-37) and cultured at 37 °C, 5% CO_2, in
328 Eagle's MEM supplemented with 20% of fetal bovine serum (FBS). To generate polarized monolayers, ~1 x10^5
329 cells were seeded onto polystyrene membrane filters (0.4µM, 6.5mm diameter insert, Transwell, Corning) and
330 grew for at least a week prior to toxin treatment. Media was replaced with fresh media every two days.

331 ### Toxin treatment

332 Polarized differentiated cells were treated with heat-labile toxin (LT) in differentiation medium (100 ng/mL)
333 in a volume of 700 µL at the basolateral side of the Transwell insert and 100 µL volume on the apical aspect of
334 the monolayer. Treated cells were incubated at 37° C for 18 hours and then fixed for transmission electron
335 microscopy or fluorescence microscopy, or lysed for RNA extraction (GE Healthcare, Buckinghamshire, UK). LT
336 and mutant LT (E211K, mLT) were kindly provided by Dr. John D. Clements, Tulane University, New Orleans,
337 Louisianna, USA.

338 ### RNA extraction and cDNA synthesis

339 RNA was extracted using Illustra RNAspin Mini RNA extraction kit (GE Healthcare, Buckinghamshire, UK).
340 Three biological replicates per treatment (untreated and LT treated) were submitted to Genome Technology
341 Access Center (GTAC) at Washington University in St. Louis School of Medicine for RNA-seq library
342 preparation. An Agilent Bioanalyzer was used to determine the integrity of RNA samples. cDNA was generated
343 using Superscript™ Vilo™ cDNA synthesis kit (Invitrogen by Thermo Fisher) after normalizing RNA
344 concentrations.

345 ### RNA-seq Library Preparation

346 Library preparation was performed with 10 ng of total RNA, integrity was determined using an Agilent
347 bioanalyzer. ds-cDNA was prepared using the SMARTer Ultra Low RNA kit for Illumina Sequencing (Clontech)
348 per manufacturer's protocol. cDNA was fragmented using a Covaris E220 sonicator using peak incident power
349 18, duty factor 20%, cycles/burst 50, time 120 seconds. cDNA was blunt ended, had an A base added to the
350 3'ends, and then had Illumina sequencing adapters ligated to the ends. Ligated fragments were then amplified
351 for 12-15 cycles using primers incorporating unique index tags. Fragments were sequenced on an Illumina
352 HiSeq-2500 using single reads extending 50 bases.

353 ### RNA-seq data processing and analysis

354 RNA-seq reads were aligned to the Ensembl top-level human genome assembly with STAR version
355 2.7.3a. Gene counts were derived from the number of uniquely aligned unambiguous reads by
356 Subread:featureCount version 1.54.1. Read counts were used as input for DESeq2 differential gene expression
357 analysis (version 1.24.0)[77] with default settings, and a minimum *P*-value significance threshold of 10^{-5} (after
358 False Discovery Rate [FDR[78]] correction for the number of tests). Fragments per kilobase per million reads
359 mapped (FPKM) values for relative gene expression were calculated from DESeq2-normalized read counts, and
360 Z-scores were calculated per gene using the average and standard deviations of FPKM values across samples.
361 Log_2 fold changes were identified from DESeq2 differential expression output. Pathway enrichment analysis for
362 KEGG[79] and Gene Ontology (GO)[80] pathways among gene sets of interest was performed using the over-
363 representation analysis tool provided on the WebGestalt[43] web server (version 2019). Heatmap and bar graph
364 visualization was performed with Microsoft Excel.

365 Transcript counts were produced by Sailfish version 0.6.3. Sequencing performance was assessed for total
366 number of aligned reads, total number of uniquely aligned reads, genes and transcripts detected, ribosomal
367 fraction known junction saturation and read distribution over known gene models with RSeQC version 2.3.

368 All gene-level and transcript counts were then imported into the R/Bioconductor package EdgeR and TMM
369 normalization size factors were calculated to adjust for samples for differences in library size. Ribosomal
370 features as well as any feature not expressed in at least the smallest condition size minus one sample were
371 excluded from further analysis and TMM size factors were recalculated to created effective TMM size factors.
372 The TMM size factors and the matrix of counts were then imported into R/Bioconductor package Limma and
373 weighted likelihoods based on the observed mean-variance relationship of every gene/transcript and sample
374 were then calculated for all samples with the voomWithQualityWeights function. Performance of the samples
375 was assessed with a spearman correlation matrix and multi-dimensional scaling plots. Gene/transcript
376 performance was assessed with plots of residual standard deviation of every gene to their average log-count

with a robustly fitted trend line of the residuals. Generalized linear models were then created to test for gene/transcript level differential expression. Differentially expressed genes and transcripts were then filtered for FDR adjusted p-values less than or equal to 0.05.

The biological interpretation of the large set of features found in the Limma results were then elucidated for global transcriptomic changes in known Gene Ontology (GO) and KEGG terms with the R/Bioconductor packages GAGE and Pathview. Briefly, GAGE measures for perturbations in GO or KEGG terms based on changes in observed $\log_2$ fold-changes for the genes within that term versus the background $\log_2$ fold-changes observed across features not contained in the respective term as reported by Limma. For GO terms with an adjusted statistical significance of FDR <= 0.05, heatmaps were automatically generated for each respective term to show how genes co-vary or co-express across the term in relation to a given biological process or molecular function. In the case of KEGG curated signaling and metabolism pathways, Pathview was used to generate annotated pathway maps of any perturbed pathway with an unadjusted statistical significance of p-value <= 0.05. Genes significantly modulated in both Caco-2 cells and enteroids were subjected to further ontology-free analysis via CompBio v1.4 (PercayAI, Inc., www.percayai.com/compbio)[81] to identify unifying biological themes in sets of genes differentially expressed between pairwise comparisons of different groups.

Quantitative real time PCR

Quantitative real time PCR was performed using a QuantStudio 3 real-time detection system (Applied Biosystems). Fast SYBR Green master mix (Applied Biosystems / Thermo Fisher) was used for qPCR analysis. Disassociation curve analysis was performed to assess the specificity of amplification for each sample, and PCR product size was verified by agarose gel electrophoresis. Percent expression was normalized by GAPDH and analyzed using the comparative threshold cycle (Ct) method. Amplification of SLC19A3 transcripts from small intestinal enteroids was performed as recently described[82] with relative gene expression normalized to β actin.

400 HNF4a, HNFg, and SMAD4 gene expression was determined by TaqMan (ThermoFisher) using validated primer
401 and probe sets. Primers and TaqMan probes used in this study are listed in Supplemental Table 2.

402 Transcriptional reporter assays

403 To assess the impact of LT on HNF4-mediated transcription, pTR104 (GeneCopoeia) carrying 6 copies of the
404 HNF4 transcriptional response element upstream of a secreted *Gaussia* luciferase (Gluc) reporter gene was
405 transfected (FuGENE, Promega) into confluent Caco-2 cells. Media (EMEM, ATCC) were exchanged 24 hours
406 after transfection, and after an additional 24 hours baseline samples of media were removed from each well
407 and stored at -80°C. Wells were then treated with heat labile toxin (100 ng/ml) overnight (16 hours). At the end
408 of treatment cell culture supernatants media were transferred to black walled microplates (Greiner 655086) and
409 processed as directed (Secrete-Pair Luminescence, GeneCopoeia, Inc. Rockville, MD), followed by
410 luminescence detection (Synergy H1, BioTek). Data are expressed as Relative Light Units (RLU) before and
411 after treatment with LT.
412 SMAD4-mediated transcription was assessed by transient transfection of Caco-2 cells with the SBE4-luc
413 plasmid containing 4 copies of the SMAD4 transcriptional response element 5'-GTCTAGAC-3'[83].
414 Following treatment with overnight treatment with LT cells were resuspended in 80 µl of EMEM media and
415 mixed with an equal volume of ONEGLO EX Reagent (Nano-Glo® Dual-Luciferase® Reporter Assay System,
416 Promega) for 20 minutes on an orbital shaker at 300 rpm, then read on the luminometer as above.

417 Immunoblotting

418 SLC19A3, SP1

419 Total protein was extracted from LT toxin-treated (100ng/ml) human differentiated enteroid monolayers (235D
420 line) and untreated control using radioimmunoprecipitation assay (RIPA) buffer (Sigma) containing protease
421 inhibitor cocktail. An equal amount (~25 µg) of the proteins were loaded on a NuPAGE 4-12% Bris–Tris gradient
422 gels (Invitrogen) as previously described[82], then blotted onto polyvinylidene difluoride (PVDF) membranes and
423 probed with anti-SLC19A3 (1:1000; Cat# 13407-1-AP; Proteintech), or anti-SP1 (1:1000; Cat# ab124804; Abcam)

antibodies and together with anti-beta actin (1:3000; Cat# sc-47778) primary antibodies. Specificity of the SLC19A3 antibodies was validated in our laboratory previously using different approaches that include overexpression of tagged protein or gene silencing[84]. Anti-SP1 antibodies were validated by the manufacturer using knockout cell lysate protein samples. The SLC19A3 and SP1 protein bands from the blot were then identified with corresponding anti-rabbit IR-800 dye (1:30,000; Cat# 926-32211; LI-COR Bioscience) and anti-mouse IR-680 dye (1:30,000; Cat# 926-68020; LI-COR Bioscience) secondary antibodies incubation for 1 h at room temperature. Relative expression of specific proteins was calculated by comparing the fluorescence intensities in an Odyssey infrared imaging system (LI-COR Bioscience) with respect to corresponding beta actin signal.

Villin

Differentiated LT-treated and control enteroid monolayers were lysed to using NE-PER™ nuclear and cytoplasmic extraction reagent (Thermo Scientific). Cell membrane pellets were solubilized in PBS containing 1% Triton X-100 supplemented with protease inhibitor cocktail (Pierce™ protease inhibitor mini, Thermo Scientific). Equal amounts of total protein were loaded on a 4-20% gradient SDS-PAGE gel (Mini Protean TGX, Bio-Rad), then blotted onto nitrocellulose membranes and probed with anti-villin mouse monoclonal antibody (1:1000; Cat# SC-66022; Santa Cruz Biotechnoogy) followed by detection with HRP-conjugated anti-mouse secondary antibody (1:1000; Cat# 7076S; Cell Signaling Technology). Blots were developed with Clarity Western ECL substrate (Bio-Rad) and imaged with c600 imaging system (Azure Biosystems). Relative Villin expression signals were then analyzed with respect to corresponding Coomassie stained gel using imageJ analysis software.

Thiamin Uptake

Initial rates (30 min; at 37 °C) of carrier-mediated thiamin uptake were examined in LT-treated (100 ng/ml; overnight) and untreated control differentiated small intestinal enteroid monolayers incubated in Krebs–Ringer buffer (pH 7.4) containing [^{3}H]-thiamin (15 nM). Enteroid monolayers were then washed with ice-cold Krebs–

448 Ringer buffer followed by lysis with NaOH and neutralization with 10 N HCl. The radioactive content was
449 counted using a liquid scintillation counter as described previously[82]. Uptake of thiamin by its respective and
450 distinct carrier-mediated mechanism was determined by subtracting uptake of [^{3}H]-thiamin in the presence of a
451 high pharmacological concentration (1 mM) of unlabeled thiamin from uptake in their absence; all uptake data
452 points were calculated relative to total protein content (in milligrams) of the different preparations and
453 presented as percentage relative to simultaneously performed controls.

454 **Confocal microscopy**

455 Cell monolayers were fixed with 2% paraformaldehyde for 30 min at 37 °C and then washed 3× with PBS prior to
456 blocking with 1% BSA in PBS for 1 h at room temperature. Villin expression was detected using 1:100 dilution of
457 anti-villin antibodies raised in mice (Santa Cruz Biotechnology) for 1 hour at room temperature followed by
458 additional 1 hour incubation with 1:200 dilution of fluorescence-tagged goat anti-mouse IgG Alexa Fluor 488
459 (Thermofisher) (Supplemental Table 5). Cell membranes were stained with 1:2000 dilution of CellMask orange
460 (Invitrogen) and nuclei were counterstained with DAPI (1:1000) and mounted on glass slides using Prolong Gold
461 antifade reagent (Invitrogen). Images were captured and analyzed on a Nikon C2 confocal microscope
462 equipped with NIS-Elements AR 5.11.01 software (Nikon).

463 **Electron Microscopy**

464 For ultrastructural analyses, *in vitro* grown differentiated polarized monolayers of human ileal enteroid samples
465 as well as mouse intestinal biopsy samples were fixed in 2% paraformaldehyde/2.5% glutaraldehyde (Ted Pella,
466 Inc., Redding, CA) in 100 mM sodium cacodylate buffer, pH 7.2 for 2 hours at room temperature and then
467 overnight at 4°C. Samples were washed in sodium cacodylate buffer and postfixed in 2% osmium tetroxide
468 (Ted Pella, Inc) 1 hour at room temperature. Samples were then rinsed in dH_2o, dehydrated in a graded series
469 of ethanol, and embedded in Eponate 12 resin (Ted Pella, Inc.). Sections of 95 nm were cut with a Leica
470 Ultracut UCT ultramicrotome (Leica Microsystems Inc., Bannockburn, IL), stained with uranyl acetate and lead
471 citrate, and viewed on a JEOL 1200 EX transmission electron microscope (JEOL USA Inc., Peabody, MA)

472 equipped with an AMT 8 megapixel digital camera and AMT Image Capture Engine V602 software (Advanced
473 Microscopy Techniques, Woburn, MA). Images were analyzed using ImageJ software for microvilli length and
474 structures.
475

476 ### Identification of potential transcription factor target sites

477 The CREB targets database[66] (http://natural.salk.edu/CREB/) was used to identify potential categorical CRE
478 full (TGACGTCA) or half (TGACG/CGTCA) sites within the promotor regions of genes modulated by heat-labile
479 toxin. Following previously described protocol[23], 5 kilobase upstream sequences from each human gene were
480 retrieved from Ensembl[85] and were searched for the CREB binding sites TGACGTCA and TGACGTAA (and their
481 reverse complements), based on sequences retrieved from the TRANSFAC[86] database (matrix ID: V$CREB_01).
482 CREB sequences matches were identified in the upstream sequences of 1,302 genes. WebGestalt[87] was used for
483 overall functional enrichment of potential transcription factor binding sequences upstream from genes that
484 were significantly ($p<0.05$) up- and down-regulated in both Caco-2 cells and enteroids.
485

486 ### Suckling mouse challenge studies

487 Studies in mice were performed under protocol 20-0438 approved by the Washington University in Saint
488 Louis Institutional Animal Care and Use Committee. In neonatal mouse challenge studies, 3-day-old CD-1 mice
489 (male and female) were inoculated with wild type ETEC (H10407), isogenic toxin deletion mutants, or sterile
490 PBS (sham negative controls). Inocula were prepared from frozen glycerol stocks maintained at -80°C grown
491 overnight (~16 hours) in 2 ml Luria Bertani (LB) broth in a shaking incubator (at 37°C, 225 rpm). Cultures were
492 then diluted 1:100 in 20 ml of fresh LB, grown for additional 2 hours, and bacteria harvested by centrifugation
493 (6000 rpm, 5 minutes at 4°C). Pellets were then washed once in ice-cold sterile PBS, then resuspended to a
494 density of ~$1*10^5$ Colony forming units (CFU) per 20 µl inoculum. CFU in each inoculum were determined by
495 plating serial dilutions LB-agar plates. Mice were then inoculated with ETEC directly into the stomach through

496 the abdominal wall using a 31g insulin needle. Following infection, mice were marked with tattoo ink to define
497 groups and returned to the cage. Seven days post infection mice were sacrificed, and the ileal tissue collected
498 fixed for microscopy, or preserved for RNA extraction.

499 Bacterial strain construction

500 Strains used in these studies are described in supplemental table 1. Strain jf4763 is devoid of all enterotoxins
501 and was constructed from a previously engineered ST-negative mutant of H10407, jf2848[88]. Briefly, jf2848 was
502 first transformed with pKD46, a lambda red recombinase helper plasmid with selection on ampicillin.
503 Jf2848(pKD46) was then transformed with a PCR amplicon generated with primers _to replace the *eltAB* genes
504 encoding LT with a spectinomycin resistance cassette resulting in jf4763. The strain was subsequently validated
505 by PCR and by testing supernatants in GM-1 ganglioside ELISA to confirm lack of LT production.

506 Vaccination and immunologic assessment

507 Adult female mouse dams were vaccinated intranasally three times at 2-week intervals with 10 µg LT holotoxin
508 in PBS, with the last dose administered approximately 2 weeks prior to anticipated delivery. Control mice were
509 mock vaccinated with PBS. Fecal pellets collected from vaccinated dams were used to assess mucosal
510 responses to LT. To collect breast milk the dam was separated from the litter ~2hours prior to milking. Oxytoxin
511 (Sigma O3251), 0.002 IU/g, was injected IP to stimulate milk production, followed by collection via pipette tip.
512 Anti-LT immune responses in maternal fecal extracts and breast milk, and stomach contents and sera of
513 neonates (male and female) were assessed by GM1 ganglioside[89] kinetic ELISA[90] for anti-LT IgA and IgG, using
514 plates coated with GM1 (Sigma G7641), as previously described[91].

515 Data availability

516 RNA seq data were deposited at the Sequence Read Archive (SRA) on the NCBI
517 website https://www.ncbi.nlm.nih.gov/sra under BioProject accession number PRJNA875141 (detail in
518 supplementary table).
519

Figures

figure 1

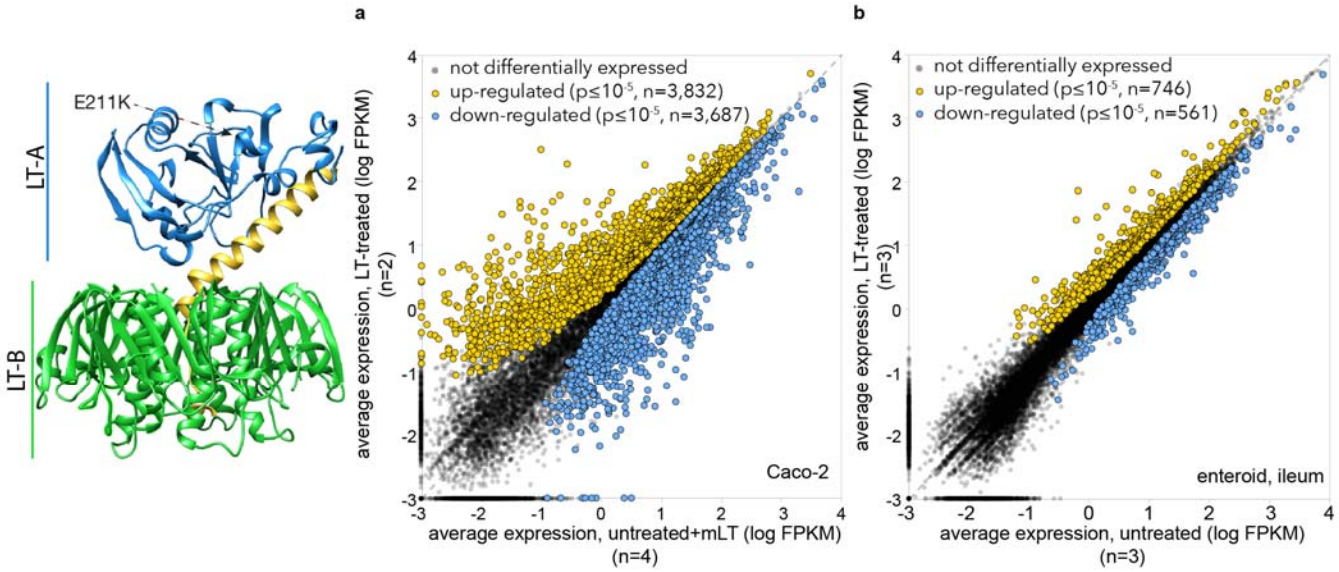

Figure 1. Heat-labile toxin modulates expression of multiple genes in intestinal epithelia. Model at left depicts the *E. coli* heat-labile toxin[92] based on PDB structure 1LTS with the A1 subunit in blue the A2 region of in yellow and pentameric B subunit in green. The E211K mutation of mLT is in the active site of the A1 subunit. **A.** Scatterplot of RNAseq data right depicts differential expression profiles of Caco-2 cells following exposure to heat-labile toxin (n=2) relative to untreated cells (n=2) and cells treated with the biologically inactive mLT (n=2). (Because expression profiles of untreated and mLT-treated cells were virtually identical**,** their combined expression profiles totaling n=4 replicates are compared here to LT-treated cells). **B.** RNAseq data from polarized small intestinal ileal enteroids treated with LT (n=3) compared to control untreated (n=3) cells.

figure 2

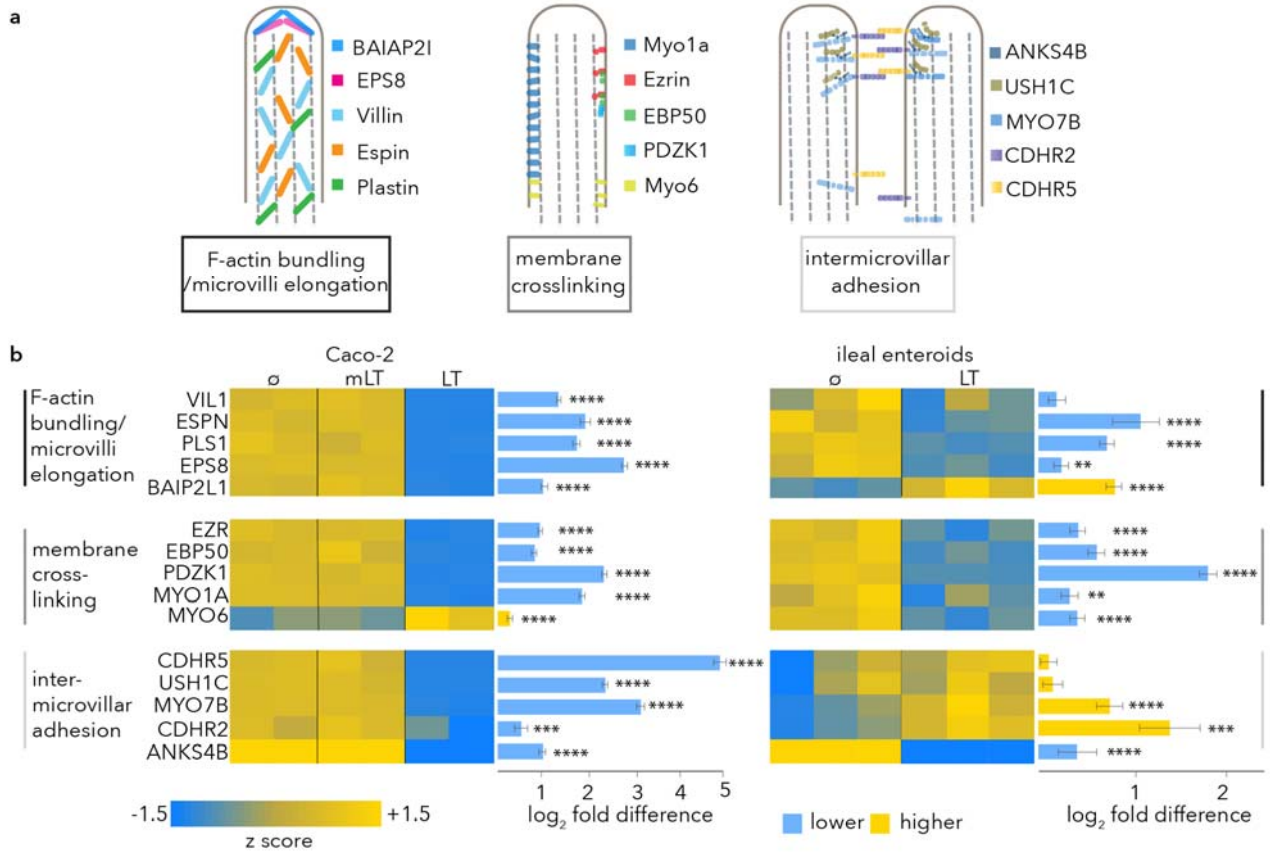

Figure 2. Heat labile toxin modulates multiple genes involved in microvillus assembly.

a. diagram at top (adapted from reference[30]) depicts molecules involved in key elements of microvillus development. **b.** heat maps of RNAseq data obtained following treatment of Caco-2 intestinal cells (left) with mLT (n=2), or LT (n=2) relative to untreated cells (n=2); and ileal enteroids (right) treated with LT (n=3) relative to control untreated cells (n=3). RNAseq fold change data comparisons were made with DESeq2[93]. Bars indicate absolute fold change values + SE. *p≤0.05, ** p≤0.01, *** p≤0.001, **** p≤10^{-4}, *****p≤10^{-5}.

figure 3

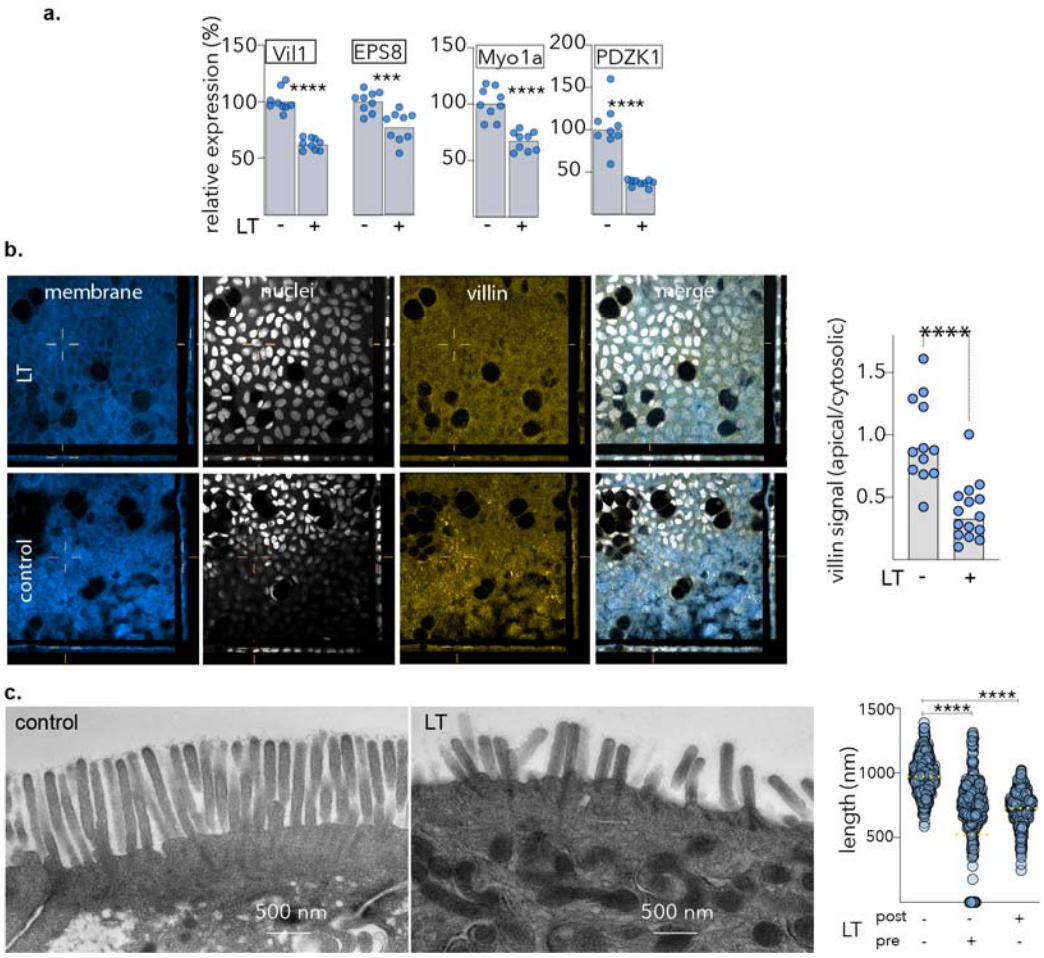

Figure 3. Heat labile toxin impairs effective formation of small intestinal microvilli.

a. quantitative RT-PCR data for selected microvillus genes comparing untreated (-) and LT-treated (+) ileal epithelial cells (enteroid line 235D). **b.** Villin production is suppressed in small intestinal enteroids following treatment (t+18h) with LT (100 µg/ml). Shown are representative confocal images obtained showing membrane (CellMask, blue), nuclei (white), villin (gold), and merged image. Graph at right shows apical villin geometric mean fluorescence intensity data relative to the corresponding cytoplasmic signal. Each symbol (n=12)represents a unique region of interest. ****p<0.0001, Mann-Whitney 2 tailed testing. **c.** TEM images of small intestinal microvilli following treatment LT (right) compared to control untreated cells (left). Graph at right shows length of microvilli when enteroids are treated before (pre) and after (post) differentiation on polarized ileal cells ****<0.0001 by ANOVA (Kruskal-Wallis, nonparametric testing).

560 figure 4

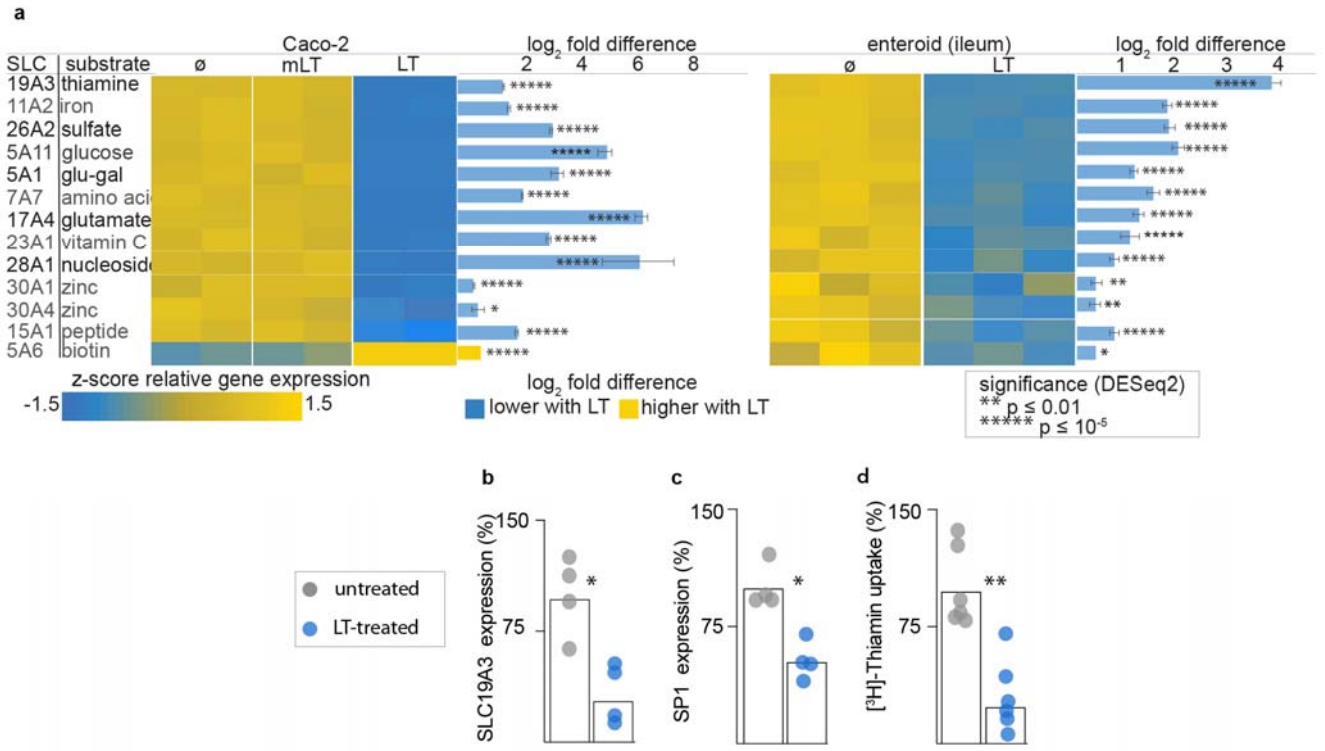

561

562 **figure 4. Heat-labile toxin alters the transcription of multiple brush border SLC genes.**

563 **a.** heat-map indicating key SLC genes modulated by heat labile toxin (LT) compared to enzymatically inactive

564 E112K LT mutant (mLT), or untreated (ø) Caco-2 cells (left) and human small intestinal (ileal) enteroids

565 (Hu235D, right). Real-time qRT-PCR confirming LT-mediated modulation of genes in ileal (Hu235D) enteroids

566 encoding (**b.**) the major thiamine transporter SLC19A3 and (**c**) the SP1 cis regulatory element. Data reflect two

567 independent experiments with 2 replicates each. **d.** uptake of [^{3}H]-thiamine by Hu235 D cells is impaired

568 following LT treatment. Data presented are from two independent experiments with n=3 replicates each. Bars

569 indicate absolute fold change values + SE (* <0.05, **<0.01 Mann-Whitney nonparametric comparisons).

570

571
572
573

figure 5.

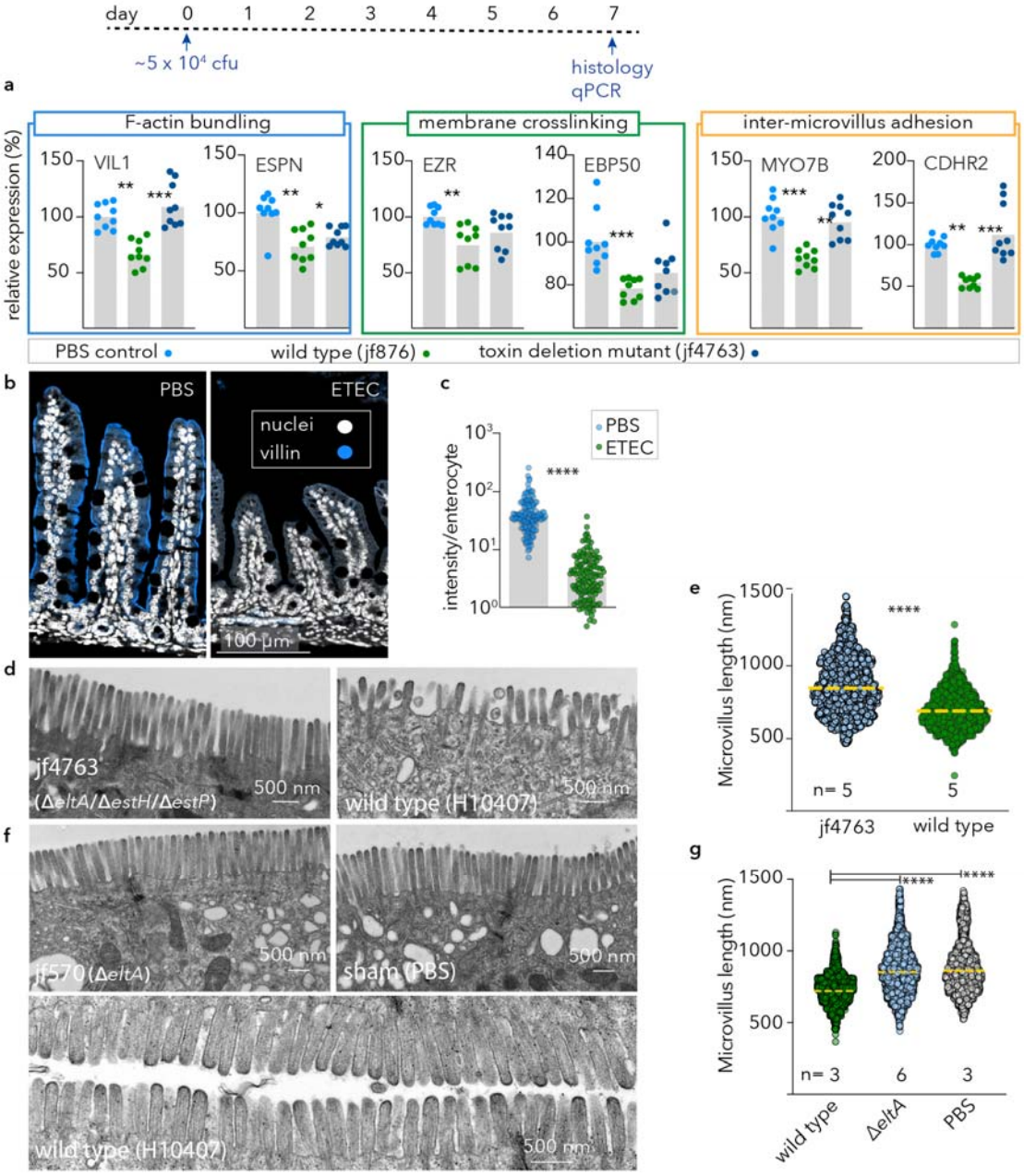

figure 5. ETEC disrupts *in vivo* formation of small intestinal microvilli

Timeline at top depicts challenge with ETEC or control nontoxigenic isolate, or sham (PBS) challenge. **a.** Quantitative PCR results for genes involved in brush border development in small intestinal samples obtained from infant mice (n=9/group) 7 days after challenge with toxigenic ETEC (jf876), nontoxigenic ETEC (jf4763, LT^-/ST^-) PBS controls. Comparisons between data represent ANOVA, Kruskal-Wallis testing where ***p≤0.001, **p≤0.01, and *p≤0.05. **b.** Immunofluorescence images of small intestinal sections showing villin expression (blue), and nuclei (white). **c.** mean villin fluorescence intensity normalized per enterocyte (n=4mice/group). **d.** representative transmission electron microscopy (TEM) images of the small intestinal brush border from mice challenged with toxin-negative (Δ, left) and toxigenic ETEC (wt, right). **e.** microvillus length ****p≤0.0001 by Mann Whitney (two-tailed) nonparametric comparisons. Data represent geometric mean length from n=5 mice

per group in three independent experiments. **f.** TEM images from mice challenged with jf570 (*eltA*::Km^R), sham PBS controls, or mice challenged with wild type ETEC. **g**. length of microvilli (dashed horizontal lines represent geometric means). ****p<0.0001 by Kruskal-Wallis.

figure 6

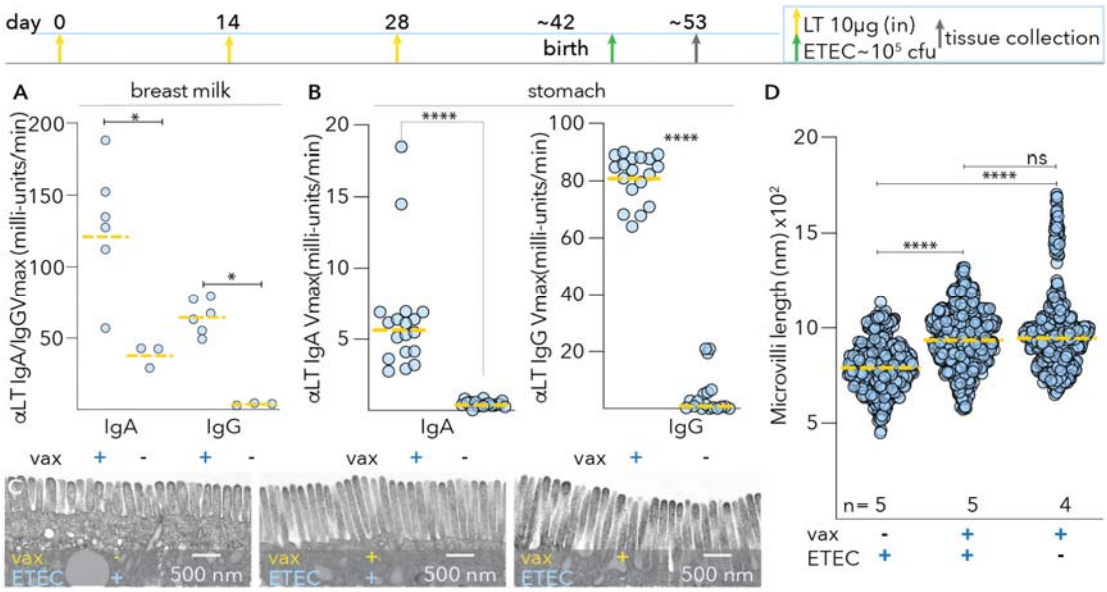

figure 6. Maternal vaccination with LT mitigates microvillus disruption in neonatal mice. Timeline depicts vaccination and challenge (top): maternal intranasal (i.n.) vaccinations with 10 µg LT/immunization (yellow arrows on days 0, 14, 28) and neonatal challenge at 3 days of age (green arrow) followed by sacrifice and tissue collection at 7 days post infection (grey arrow). **A**. Kinetic ELISA data of breast milk anti-LT (IgA, and IgG in immunized dams and un-immunized controls). *<0.05 by Mann-Whitney two-tailed nonparametric testing. **B.** Anti-LT antibodies in the gastric contents of neonatal mice at day 53. **C.** Representative transmission electron microscopy images of brush border microvilli from unvaccinated mice challenged with wild type ETEC (left), vaccinated mice challenged with wild type ETEC, and vaccinated un-challenged controls. **D.** Microvillus lengths (based on image analysis of n=5 mice group) ****<0.0001 Kruskal-Wallis comparisons.

605 **figure 7**

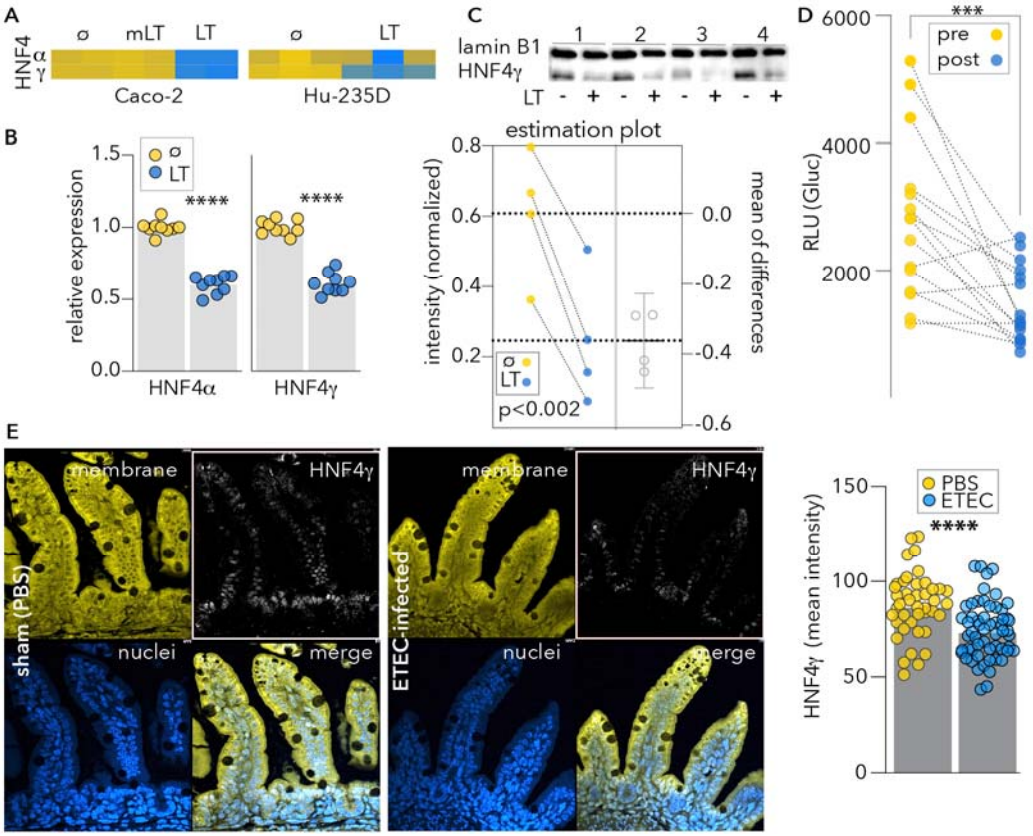

606
607
608 **Enterotoxigenic E. coli heat-labile toxin impairs production of HNF4 nuclear receptors**.
609 **A.** heatmap demonstrating the impact of LT on transcription of paralogous transcription factors HNF4α and
610 HNF4γ in Caco-2cells (left) and ileal enteroids, (Hu-235D, right) ø = untreated, mLT = mutant LT. **B.** qRT-PCR
611 (TaqMan) data confirming decreased transcription of HNF4 transcription factors following treatment of
612 enteroids with LT. **C**. HNF4γ is decreased in nuclear fractions obtained from small intestinal enteroids following
613 treatment with LT. Shown in the HNF4γ immunoblot are samples from 4 independent experiments with graph
614 below representing quantitation of signal intensity normalized to the lamin B1 nuclear protein (p=0.0017, paired
615 t-test, one-tailed). **D.** HNF4 transcription *Gaussia* luciferase reporter assay showing decrease in signal following
616 treatment of TR104-transfected Caco-2 cells with LT. 2 experimental replicates (n=15 samples total) ***
617 p<0.001 Wilcoxon matched pairs, one-tailed). **E.** Confocal microscopy of representative Ileal sections from
618 sham-challenged (PBS) left, and ETEC-infected mice (right). Immunofluorescence intensity of HNF4γ signal in
619 sections from n=5 control mice, and n=6 ETEC-challenged mice. Membranes (yellow) were strained with
620 CellMask orange (ThermoFisher C10045), nuclei (blue) stained with DAPI, and HNFγ immunostaining
621 represented in white. Each symbol represents a microscopic region of interest. Bars represent geographic
622 means (p<0.0001, Mann-Whitney two-tailed comparisons).
623

Supplemental Data

Supplemental Figures

supplemental figure 1

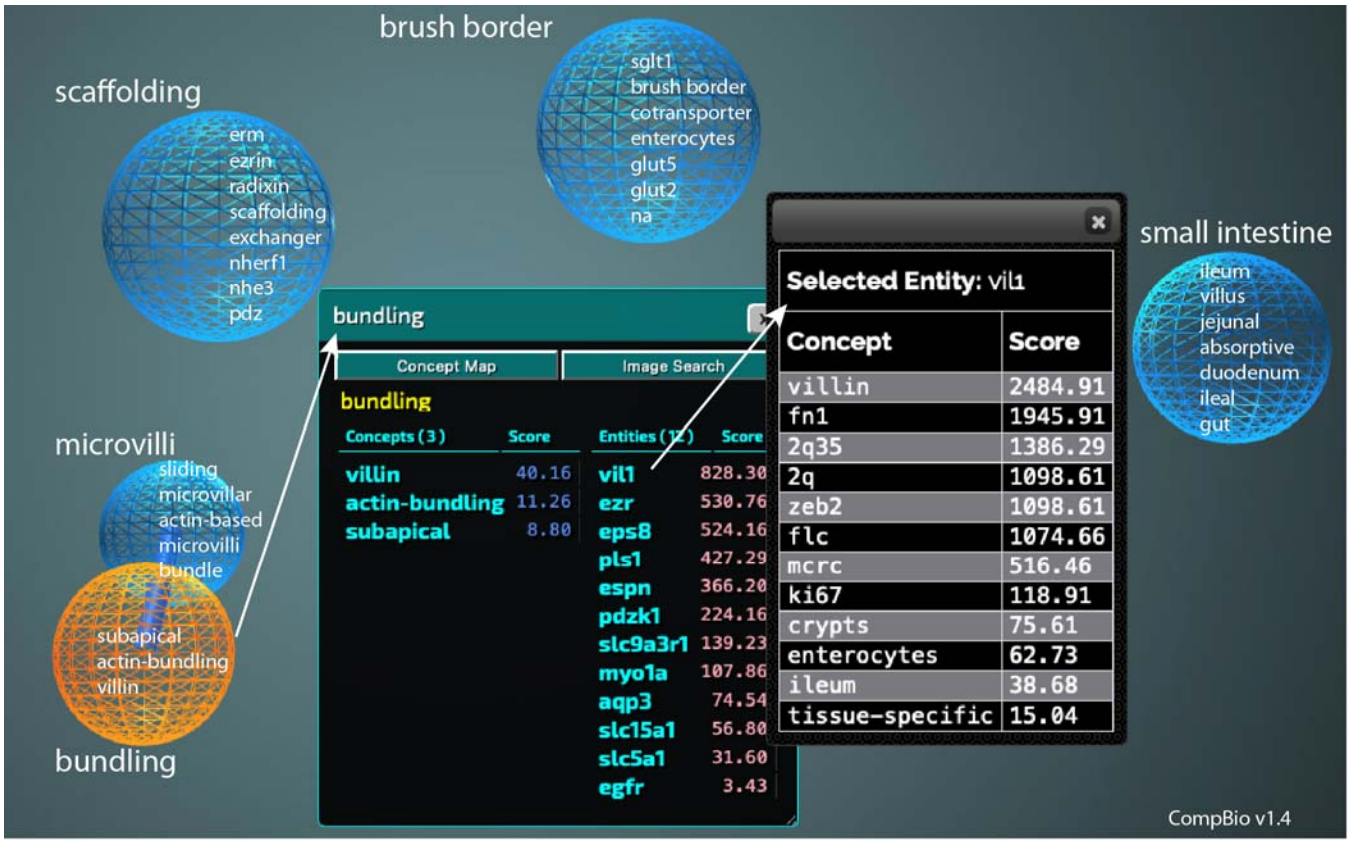

Supplemental figure 1. image from representative CombBio (v1.4) analysis of differential gene expression in LT-treated enteroids compared to untreated controls, highlighting themes (spheres) related to biogenesis and function of small intestinal microvilli. Concepts linked within each theme are listed on the corresponding sphere.

633 **Supplemental figure 2**

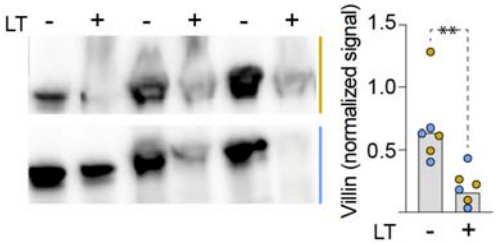

634

635 **Supplemental figure 2. Villin production is decreased in LT-treated small intestinal enteroids.** Shown are
636 villin immunoblot signals in membrane preparations from 2 independent experiments (coded by color), each
637 with 3 technical replicates. LT+ indicates overnight ~16 h treatment of ileal enteroids with heat-labile toxin [100
638 µg/ml]. Graph summarizes villin immunoblot signals normalized to total protein. (**p=0.0043 Mann Whitney,
639 two-tailed comparisons).

640

641

642 **supplemental figure 3**

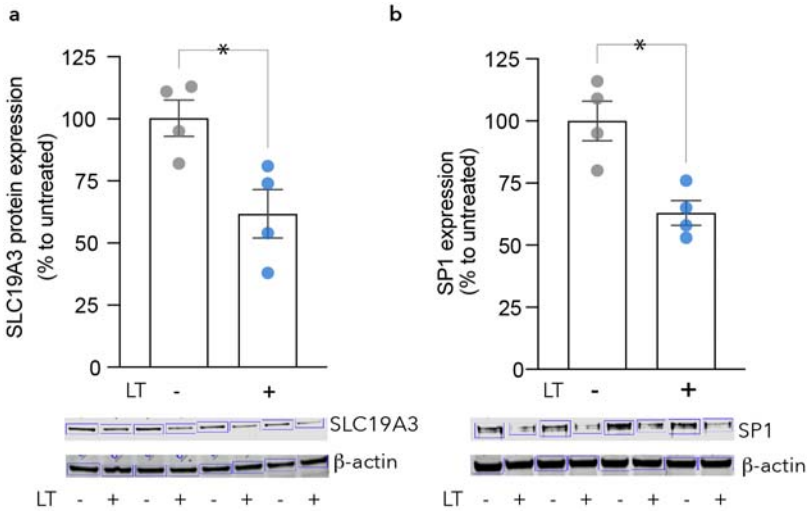

643

644 **Supplemental figure 3. Impact of LT on expression of SLC19A3 and its associated SP1 transcription factor.**

645 Graphs depict summary of immunoblot band intensities of SLC19A3 (**a**) and the SP1 transcription factor (**b**)

646 generated on probing LT-treated small intestinal enteroids (235D) relative to untreated controls. *<0.05 by

647 Mann Whitney two-tailed analysis. Bars reflect geometric mean data ± SEM. The corresponding immunoblots

648 from 4 independent experimental replicates are shown below each graph.

649

650

supplemental figure 4

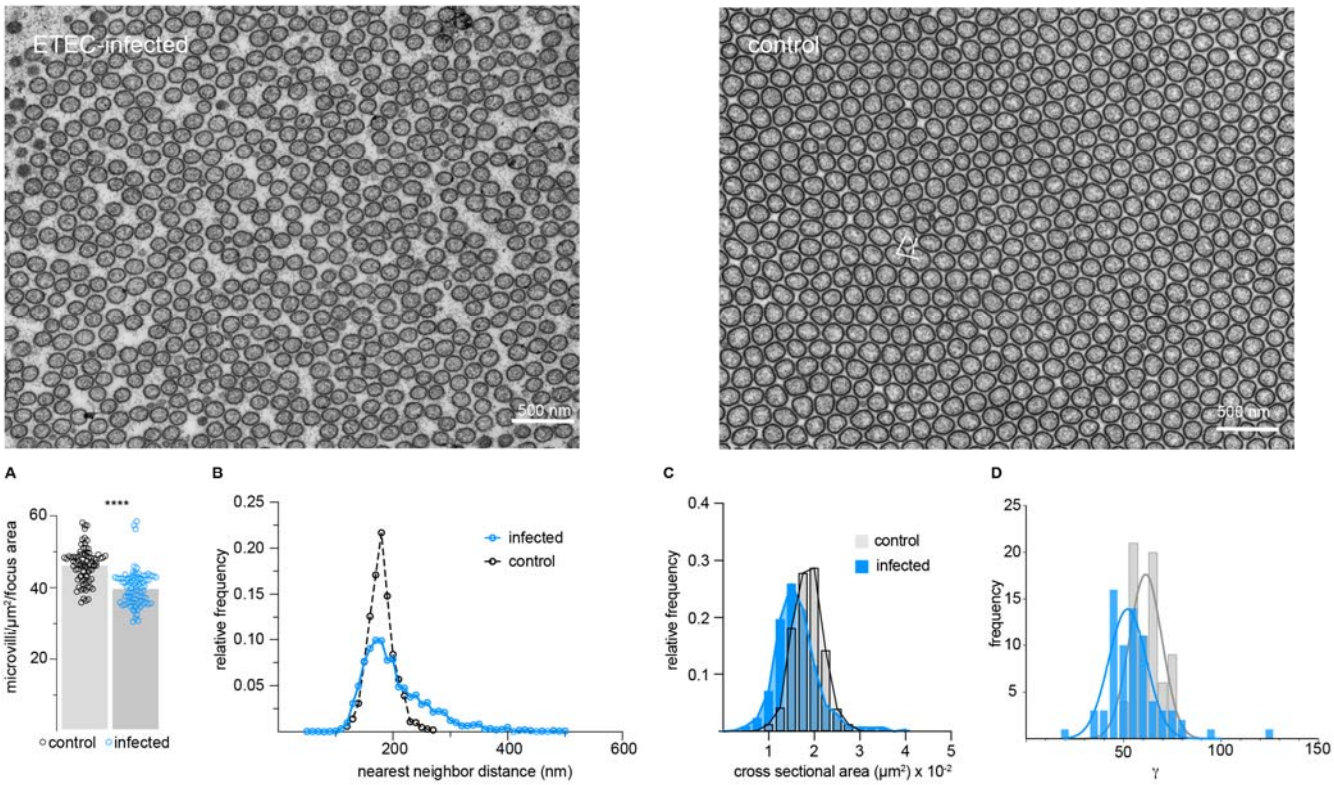

Supplemental figure 4. ETEC perturbs the ordered array structure of intestinal microvilli. Shown at top are representative TEM cross sections of infected and control mice (n=5) in each group. **A.** density of microvilli/µm² (n=83 areas in infected and control). p<0.0001. **B.** distance between centers of adjacent microvilli (n=1001 control, n=2278 infected), p<0.0001 Mann-Whitney. **C.** cross sectional area of microvilli (n=550 control, n=1559 infected) p<0.0001. **D.** g angle distributions of microvilli from control and ETEC-infected mice. (analysis by Mann-Whitney, 2-tailed, nonparametric comparisons).

662
663 supplemental figure 5.

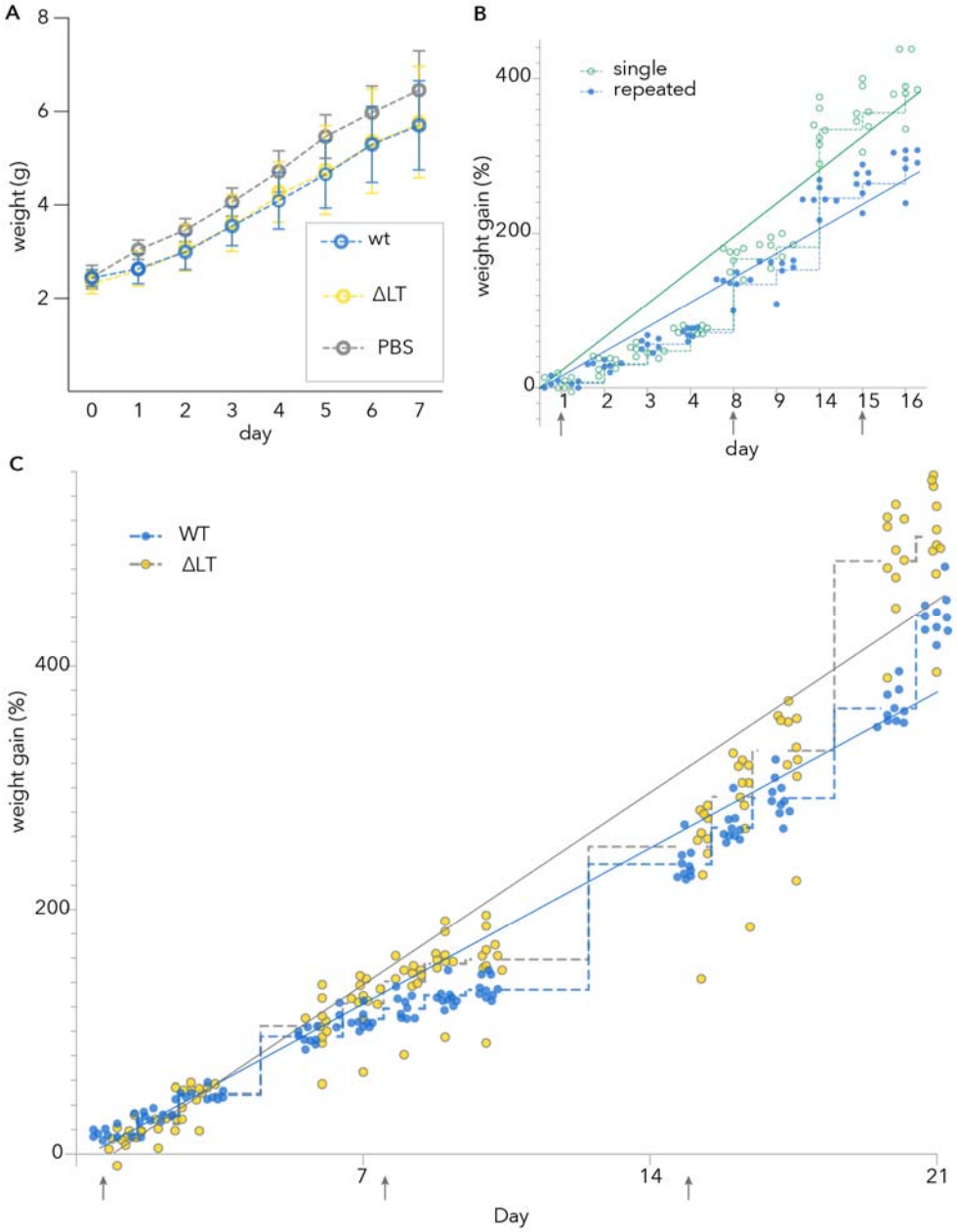

664
665 **Supplemental figure 5. growth kinetics following challenge of suckling mice with ETEC**
666 **A.** Short-term growth kinetics of mice singly challenged with wild type toxigenic ETEC H10407 (WT), LT mutant
667 (*ΔeltA*, jf571), vs sham challenge (PBS) (n=24/group). data points reflect mean ± sd. **B.** Repeated vs single challenge
668 of mice with wild type toxigenic ETEC H10407 (wt) (n=7 mice/group); dashed lines connect geometric mean values.
669 Solid lines = linear regression. Comparison between singly and repeatedly infected by two-way ANOVA p=0.0004) **C.**
670 LT contributes to growth impairment on repeated challenge. Shown are mice (n=10/group) repeatedly challenged
671 with either H10407 or the LT deletion mutant jf571. Stepped lines connect geometric mean values. Solid lines
672 indicate linear regression. (Comparison between WT and ΔLT by two-way ANOVA p=0.0078).
673

674 **supplemental figure 6**

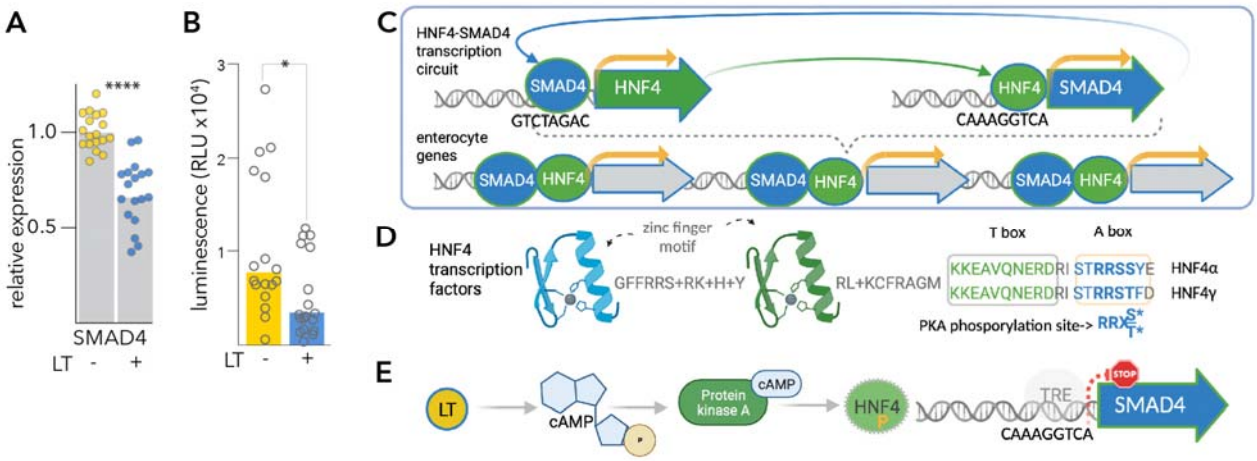

675
676 **Supplemental figure 6.** Potential mechanism underlying LT mediated disruption of brush border development.
677 LT interrupts HNF4-SMAD4 mediated transcription. **A.** treatment of human-derived small intestinal enteroids
678 (Hu235D) with LT leads to decreased SMAD4 transcription. Shown are TaqMan probe results from two independent
679 experiments of polarized epithelial monolayers treated with LT. n=3 biological replicates x 3 technical replicates/
680 experiment =18 data points. ****p<0.0001 by Mann Whitney, two-tailed nonparametric comparisons to untreated
681 cells. **B.** SMAD4-mediated transcription is decreased by LT. Shown are the combined results of three independent
682 experiments in which Caco-2 cells transiently transfected with the SBE4-Luc plasmid containing 4 copies of the
683 SMAD4 transcriptional response element were treated with LT (100 µg/ml x 16 hours). *=0.015 (Mann-Whitney). **C.**
684 depiction of the HNF4-SMAD4 reciprocal transcription factor activation in which HNF4 activates transcription of
685 SMAD4 and *vice versa* as (Chen, *et* al[71]). **D.** PKA-mediated phosphorylation of HNF4 paralogs interrupts a DNA-
686 binding module (Viollet, *et al*[70].). **E.** Summary of proposed mechanism by which LT leads to depletion of transcription
687 factors essential for enterocyte differentiation. LT-mediated activation of PKA leads to phosphorylation of HNF4
688 rendering these transcription factors incapable of binding to *cis* transcriptional response elements (TRE) in
689 promotors of target genes including SMAD4. Decreased SMAD4 transcription in turn depletes available HNF4.
690

691
692 ## Supplemental Tables
693 **supplemental table 1**

strains and plasmids used in these studies		
bacterial strains		
strain designation	description	source
H10407	wild type ETEC strain, *eltAB*, *estP*, *estH*	[94]
jf570	*Δ eltAB* derivative of H10407	[95]
jf876	*lacZYA*::Km^R derivative of H10407	[95]
jf4763	*eltAB*::Sp^R, estP::Km^R, estH::Cm^R toxin-negative derivative of H10407.	this study
plasmids		
designation	description	source
TR104	6 copies of HNF4 transcriptional response element upstream of Gaussia luciferase reporter (Gaussia-Dura Luc). Km^R, Pm^R	GeneCopoeia
SEAP-PA01	secreted alkaline phosphatase; CMV promotor; Amp^R	GeneCopoeia
SBE4-Luc	Luciferase reporter containing four copies of the SMAD4 binding site. 5'-GTCTAGAC-3'	addgene [83]

Sp^R spectinomycin resistant; Km^R kanamycin resistant; Cm^R chloramphenicol resistant; Pm^R puromycin resistant, Amp^R ampicillin resistant

694
695

696
697 **supplemental table 2 primers and probes for gene expression**

RT-PCR primers			
gene	species	primer sequence (5'-3')	
		forward	reverse
SLC19A3	Human	TTCCTGGATTTACCCCACTG	TATGTCCAAACGGGGAAGA
VIL1	Human	CTGAGCGCCCAAGTCAAAG	AGCAGTCACCATCGAAGAAGC
MYO1A	Human	ACAGGCGAGAGTGGATCAG	GCACTGGGTTAGACTGTAGCAG
MYO7B	Human	TGGACGCCTCAGACGTGAT	CTGGTGACAAATTCCCCTCGG
SP-1	Human	CCATACCCCTTAACCCCG	GAATTTTCACTAATGTTTCCCACC
GAPDH	Human	CATTTCCTGGTATGACAACGA	CTTCCTCTTGTGCTCTTGCT
b-actin	Human	CATCCTGCGTCTGGACCT	TAATGTCACGCACGATTTCC
Ezr	Mouse	CAATCAACGTCCGGGTGAC	GCCAATCGTCTTTACCACCTGA
Vil1	Mouse	TCAAAGGCTCTCTCAACATCAC	AGCAGTCACCATCGAAGAAGC
Espn	Mouse	GGAAATACAGAGGGCGAAAGA	AGAAGCCGAGAGACTCCTATTA
Cdhr2	Mouse	GGCCTCGATTCTACAGCCAAT	GCTCAGAGCCATTCTCAGTCAC
Myo7B	Mouse	AGGGGACCTGAATGAGGCT	GCGGCTGTAGTAGATTTGTACCT
Ebp50	Mouse	AGGGTCCAAATGGCTACGG	CTCCACCAATCGGTCTCCAG
GAPDH	Mouse	AGGTCGGTGTGAACGGATTTG	TGTAGACCATGTAGTTGAGGTCA
TaqMan probes			
gene	species	chromosome	location
HNF4α	Human	20	44355801 - 44432845
HNF4γ	Human	8	75407567 - 75566834
SMAD4	Human	18	51030213 - 51085042

698

699

700

701 **supplemental table 3**

differential gene expression in gastrointestinal cells following treatment with LT			
response to LT	dataset	genes (n) $p<0.05$*	genes (n) $p<10^{-5}$*
higher	Caco-2	5,631	3,832
	ileal enteroids	2138	746
	both†	877	268
lower	Caco-2	5,263	3,687
	ileal enteroids	1,839	561
	both†	1,013	311

*differentially expressed genes identified by DESeq2[93]
† overlap in up- and downregulated genes was statistically higher than expected by random selection ($p<10^{-10}$, binomial distribution testing)
Expression values of LT-treated enteroid cells are relative to untreated cells; LT-treated Caco-2 values are relative to untreated Caco-2 cells plus those treated with mLT.

702
703

704 supplemental table 4.

supplemental table 4. Transcription factor target sequence enrichment among genes differentially regulated in both RNA-seq datasets

transcription factor target					
transcription factor	target designation	target motif	Total pathway size	Number of significant genes	FDR-adjusted P value
*877 genes upregulated by LT in both RNA-seq datasets**					
AP1 / JUN	TGANTCA_V$AP1_C	TGANTCA	1108	91	4.2E-03
LEF1	CTTTGT_V$LEF1_Q2	CTTTGT	1939	142	4.2E-03
USF	V$USF_C	NCACGTGN	278	32	5.2E-03
*1,013 genes downregulated by LT in both RNA-seq datasets**					
HNF4αγ	V$HNF4_01	NNNRGGNCAAAGKTCANNN	269	37	1.9E-04
HNF4αγ	V$HNF4_01_B	NRGGNCAAAGGTCAN	249	32	2.6E-03
USF	V$USF_02	NNRNCACGTGNYNN	270	32	8.8E-03
SREBP1	TCANNTGAY_V$SREBP1_01	TCANNTGAY	469	47	9.9E-03
NR2F2/COUP	V$COUP_01	TGAMCTTTGMMCYT	260	30	0.015
IRF1	STTTCRNTTT_V$IRF_Q6	STTTCRNTTT	185	23	0.025
USF	V$USF_01	NNRYCACGTGRYNN	254	28	0.038
HNF1	RGTTAMWNATT_V$HNF1_01	RGTTAMWNATT	72	12	0.044

705 *differentially expressed genes identified by DESeq2[93] $p<0.05$
706

707

708 **supplemental table 5.**

antibodies used in these studies		
Specificity	description	source/reference
villin	Villin antibody (BDID2C3), mouse monoclonal IgG1	Santa Cruz sc-66022
mouse IgG	Goat anti-Mouse (H&L) IgG, highly cross-adsorbed antibody conjugated to Alexa Fluor 488	ThermoFisher A-11029
mouse IgA	Pre-absorbed, affinity purified goat anti-mouse IgA conjugated to HRP	Santa Cruz sc-3793
mouse IgG	Affinity purified horse anti-mouse IgG conjugated to HRP	Cell Signaling 7076
HNF4γ	rabbit polyclonal IgG against residues 327-408 of human HNF4γ	ThermoFisher 25801-1-AP
HNF4α	monoclonal IgG2a clone K9218) vs Baculovirus-expressed recombinant human HNF4α (aa 3-49)	ThermoFisher MA1-199
SP-1	rabbit monoclonal against synthetic peptide within Human SP1 aa 550-650.	abcam ab124804
SLC19A3	rabbit polyclonal IgG vs SLC19A3	proteintech 13407-1-AP
β-actin	β-Actin (C4) is a mouse monoclonal antibody (IgG1 kappa light chain) raised against gizzard Actin of chicken origin.	Santa Cruz sc-47778
rabbit IgG	IRDye® 800CW Goat anti-Rabbit IgG Secondary Antibody	LiCor 926-32211
mouse IgG	IRDye® 680LT Goat anti-Mouse IgG Secondary Antibody	LiCor 926-68020

709

supplemental table 6

links to original images	
item	DOI
figure 4b	10.6084/m9.figshare.19251848
figure 4c	10.6084/m9.figshare.19251845
figure 5b	10.6084/m9.figshare.19287353
figure 5e	10.6084/m9.figshare.19251911
figure 5g	10.6084/m9.figshare.19251926
figure 6c	10.6084/m9.figshare.19251938
figure 7c	10.6084/m9.figshare.19742413
supplemental figure 2	10.6084/m9.figshare.21217775
supplemental figure 3a	10.6084/m9.figshare.21217721
supplemental figure 3b	10.6084/m9.figshare.21217712

References

1 Collaborators, G. B. D. D. D. Quantifying risks and interventions that have affected the burden of diarrhoea among children younger than 5 years: an analysis of the Global Burden of Disease Study 2017. *Lancet Infect Dis* **20**, 37-59 (2020). https://doi.org:10.1016/S1473-3099(19)30401-3

2 Sack, R. B. *et al.* Enterotoxigenic Escherichia coli isolated from patients with severe cholera-like disease. *J Infect Dis* **123**, 378-385 (1971).

3 Kotloff, K. L. *et al.* Burden and aetiology of diarrhoeal disease in infants and young children in developing countries (the Global Enteric Multicenter Study, GEMS): a prospective, case-control study. *Lancet* **382**, 209-222 (2013). https://doi.org:10.1016/S0140-6736(13)60844-2

4 Kotloff, K. L. *et al.* The incidence, aetiology, and adverse clinical consequences of less severe diarrhoeal episodes among infants and children residing in low-income and middle-income countries: a 12-month case-control study as a follow-on to the Global Enteric Multicenter Study (GEMS). *Lancet Glob Health* **7**, e568-e584 (2019). https://doi.org:10.1016/S2214-109X(19)30076-2

5 Steffen, R., Hill, D. R. & DuPont, H. L. Traveler's diarrhea: a clinical review. *JAMA* **313**, 71-80 (2015). https://doi.org:10.1001/jama.2014.17006

6 Khalil, I. A. *et al.* Morbidity and mortality due to shigella and enterotoxigenic Escherichia coli diarrhoea: the Global Burden of Disease Study 1990-2016. *Lancet Infect Dis* **18**, 1229-1240 (2018). https://doi.org:10.1016/S1473-3099(18)30475-4

7 Nasrin, D. *et al.* Pathogens associated with linear growth faltering in children with diarrhea and impact of antibiotic treatment: The Global Enteric Multicenter Study. *J Infect Dis* (2021). https://doi.org:10.1093/infdis/jiab434

8 Qadri, F. *et al.* Disease burden due to enterotoxigenic Escherichia coli in the first 2 years of life in an urban community in Bangladesh. *Infect Immun* **75**, 3961-3968 (2007). https://doi.org:10.1128/IAI.00459-07

9 Black, R. E., Brown, K. H. & Becker, S. Effects of diarrhea associated with specific enteropathogens on the growth of children in rural Bangladesh. *Pediatrics* **73**, 799-805 (1984).

10 Anderson, J. D. t. *et al.* Burden of enterotoxigenic Escherichia coli and shigella non-fatal diarrhoeal infections in 79 low-income and lower middle-income countries: a modelling analysis. *Lancet Glob Health* **7**, e321-e330 (2019). https://doi.org:10.1016/S2214-109X(18)30483-2

11 Caulfield, L. E., de Onis, M., Blossner, M. & Black, R. E. Undernutrition as an underlying cause of child deaths associated with diarrhea, pneumonia, malaria, and measles. *Am J Clin Nutr* **80**, 193-198 (2004). https://doi.org:10.1093/ajcn/80.1.193

12 Checkley, W. *et al.* Multi-country analysis of the effects of diarrhoea on childhood stunting. *Int J Epidemiol* **37**, 816-830 (2008). https://doi.org:10.1093/ije/dyn099

13 Klipstein, F. A., Short, H. B., Engert, R. F., Jean, L. & Weaver, G. A. Contamination of the small intestine by enterotoxigenic coliform bacteria among the rural population of Haiti. *Gastroenterology* **70**, 1035-1041 (1976).

14 Klipstein, F. A., Holdeman, L. V., Corcino, J. J. & Moore, W. E. Enterotoxigenic intestinal bacteria in tropical sprue. *Ann Intern Med* **79**, 632-641 (1973).

15 Klipstein, F. A., Engert, R. F. & Short, H. B. Enterotoxigenicity of colonising coliform bacteria in tropical sprue and blind-loop syndrome. *Lancet* **2**, 342-344 (1978).

16 Brunser, O., Eidelman, S. & Klipstein, F. A. Intestinal morphology of rural Haitians. A comparison between overt tropical sprue and asymptomatic subjects. *Gastroenterology* **58**, 655-668 (1970).

17 Mathan, M., Mathan, V. I. & Baker, S. J. An electron-microscopic study of jejunal mucosal morphology in control subjects and in patients with tropical sprue in southern India. *Gastroenterology* **68**, 17-32 (1975).

18 Fleckenstein, J. M. *et al.* Molecular mechanisms of enterotoxigenic Escherichia coli infection. *Microbes Infect* **12**, 89-98 (2010). https://doi.org:S1286-4579(09)00235-4 [pii] 10.1016/j.micinf.2009.10.002

19 Tsai, S. C., Noda, M., Adamik, R., Moss, J. & Vaughan, M. Enhancement of choleragen ADP-ribosyltransferase activities by guanyl nucleotides and a 19-kDa membrane protein. *Proc Natl Acad Sci U S A* **84**, 5139-5142. (1987).

20 Lodish H, B. A., Zipursky SL, Matsudaira P, Baltimore D, Darnell J. in *Molecular Cell Biology* (W. H. Freeman, 2000).

21 Sassone-Corsi, P. Transcription factors responsive to cAMP. *Annu Rev Cell Dev Biol* **11**, 355-377 (1995). https://doi.org:10.1146/annurev.cb.11.110195.002035

22 Sassone-Corsi, P. The cyclic AMP pathway. *Cold Spring Harb Perspect Biol* **4** (2012). https://doi.org:10.1101/cshperspect.a011148

23 Zambon, A. C. *et al.* Gene expression patterns define key transcriptional events in cell-cycle regulation by cAMP and protein kinase A. *Proc Natl Acad Sci U S A* **102**, 8561-8566 (2005). https://doi.org:10.1073/pnas.0503363102

24 Hansson, H. A., Lange, S., Lonnroth, I., Rozell, B. & Tinberg, H. Cytoskeletal disarrangement in rat intestinal epithelium after in vivo exposure to secretagogues. *Acta Pathol Microbiol Immunol Scand [B]* **92**, 93-99 (1984).

25 Mathan, M. M., Chandy, G. & Mathan, V. I. Ultrastructural changes in the upper small intestinal mucosa in patients with cholera. *Gastroenterology* **109**, 422-430 (1995). https://doi.org:10.1016/0016-5085(95)90329-1

26 Asakura, H., Tsuchiya, M., Watanabe, Y., Enomoto, Y. & Morita, A. Electron microscopic study on the jejunal mucosa in human cholera. *Gut* **15**, 531-544 (1974). https://doi.org:10.1136/gut.15.7.531

27 Platts-Mills, J. A. *et al.* Association between enteropathogens and malnutrition in children aged 6-23 mo in Bangladesh: a case-control study. *Am J Clin Nutr* **105**, 1132-1138 (2017). https://doi.org:10.3945/ajcn.116.138800

28 Ilantzis, C., DeMarte, L., Screaton, R. A. & Stanners, C. P. Deregulated expression of the human tumor marker CEA and CEA family member CEACAM6 disrupts tissue architecture and blocks colonocyte differentiation. *Neoplasia* **4**, 151-163 (2002). https://doi.org:10.1038/sj.neo.7900201

29 Tadjali, M., Seidelin, J. B., Olsen, J. & Troelsen, J. T. Transcriptome changes during intestinal cell differentiation. *Biochim Biophys Acta* **1589**, 160-167 (2002). https://doi.org:10.1016/s0167-4889(02)00170-2

30 Crawley, S. W., Mooseker, M. S. & Tyska, M. J. Shaping the intestinal brush border. *J Cell Biol* **207**, 441-451 (2014). https://doi.org:10.1083/jcb.201407015

31 Postema, M. M., Grega-Larson, N. E., Neininger, A. C. & Tyska, M. J. IRTKS (BAIAP2L1) Elongates Epithelial Microvilli Using EPS8-Dependent and Independent Mechanisms. *Curr Biol* **28**, 2876-2888 e2874 (2018). https://doi.org:10.1016/j.cub.2018.07.022

32 Tyska, M. J. *et al.* Myosin-1a is critical for normal brush border structure and composition. *Mol Biol Cell* **16**, 2443-2457 (2005). https://doi.org:10.1091/mbc.e04-12-1116

33 Crawley, S. W., Weck, M. L., Grega-Larson, N. E., Shifrin, D. A., Jr. & Tyska, M. J. ANKS4B Is Essential for Intermicrovillar Adhesion Complex Formation. *Dev Cell* **36**, 190-200 (2016). https://doi.org:10.1016/j.devcel.2015.12.022

34 He, L., Vasiliou, K. & Nebert, D. W. Analysis and update of the human solute carrier (SLC) gene superfamily. *Hum Genomics* **3**, 195-206 (2009). https://doi.org:10.1186/1479-7364-3-2-195

35 Manary, M. J. *et al.* Perturbed zinc homeostasis in rural 3-5-y-old Malawian children is associated with abnormalities in intestinal permeability attributed to tropical enteropathy. *Pediatr Res* **67**, 671-675 (2010). https://doi.org:10.1203/PDR.0b013e3181da44dc

36 Reidling, J. C., Lambrecht, N., Kassir, M. & Said, H. M. Impaired intestinal vitamin B1 (thiamin) uptake in thiamin transporter-2-deficient mice. *Gastroenterology* **138**, 1802-1809 (2010). https://doi.org:10.1053/j.gastro.2009.10.042

37 Subramanian, V. S., Marchant, J. S. & Said, H. M. Targeting and trafficking of the human thiamine transporter-2 in epithelial cells. *J Biol Chem* **281**, 5233-5245 (2006). https://doi.org:10.1074/jbc.M512765200

38 Said, H. M., Balamurugan, K., Subramanian, V. S. & Marchant, J. S. Expression and functional contribution of hTHTR-2 in thiamin absorption in human intestine. *American journal of physiology. Gastrointestinal and liver physiology* **286**, G491-498 (2004). https://doi.org:10.1152/ajpgi.00361.2003

39 Nabokina, S. M., Subramanian, V. S., Valle, J. E. & Said, H. M. Adaptive regulation of human intestinal thiamine uptake by extracellular substrate level: a role for THTR-2 transcriptional regulation. *American journal of physiology. Gastrointestinal and liver physiology* **305**, G593-599 (2013). https://doi.org:10.1152/ajpgi.00237.2013

40 Nabokina, S. M. & Said, H. M. Characterization of the 5'-regulatory region of the human thiamin transporter SLC19A3: in vitro and in vivo studies. *Am J Physiol Gastrointest Liver Physiol* **287**, G822-829 (2004). https://doi.org:10.1152/ajpgi.00234.2004

41 Nabokina, S. M., Reidling, J. C. & Said, H. M. Differentiation-dependent up-regulation of intestinal thiamin uptake: cellular and molecular mechanisms. *J Biol Chem* **280**, 32676-32682 (2005). https://doi.org:10.1074/jbc.M505243200

42 Checkley, W. *et al.* Multi-country analysis of the effects of diarrhoea on childhood stunting. *Int J Epidemiol* **37**, 816-830 (2008). https://doi.org:10.1093/ije/dyn099

43 Wang, J., Vasaikar, S., Shi, Z., Greer, M. & Zhang, B. WebGestalt 2017: a more comprehensive, powerful, flexible and interactive gene set enrichment analysis toolkit. *Nucleic Acids Res.* **45**, W130-W137 (2017). https://doi.org:10.1093/nar/gkx356

44 Liberzon, A. *et al.* The Molecular Signatures Database (MSigDB) hallmark gene set collection. *Cell Syst* **1**, 417-425 (2015). https://doi.org:10.1016/j.cels.2015.12.004

45 Nakamura, T., Datta, R., Sherman, M. L. & Kufe, D. Regulation of c-jun gene expression by cAMP in HL-60 myeloid leukemia cells. *J Biol Chem* **265**, 22011-22015 (1990).

46 Wang, P. Y. *et al.* c-Jun enhances intestinal epithelial restitution after wounding by increasing phospholipase C-gamma1 transcription. *Am J Physiol Cell Physiol* **312**, C367-C375 (2017). https://doi.org:10.1152/ajpcell.00330.2016

47 San Roman, A. K., Aronson, B. E., Krasinski, S. D., Shivdasani, R. A. & Verzi, M. P. Transcription factors GATA4 and HNF4A control distinct aspects of intestinal homeostasis in conjunction with transcription factor CDX2. *J Biol Chem* **290**, 1850-1860 (2015). https://doi.org:10.1074/jbc.M114.620211

48 Chen, L. *et al.* The nuclear receptor HNF4 drives a brush border gene program conserved across murine intestine, kidney, and embryonic yolk sac. *Nature communications* **12**, 2886 (2021). https://doi.org:10.1038/s41467-021-22761-5

49 Dankel, S. N., Hoang, T., Flageng, M. H., Sagen, J. V. & Mellgren, G. cAMP-mediated regulation of HNF-4alpha depends on the level of coactivator PGC-1alpha. *Biochim Biophys Acta* **1803**, 1013-1019 (2010). https://doi.org:10.1016/j.bbamcr.2010.05.008

50 Khalil, I. *et al.* Enterotoxigenic Escherichia coli (ETEC) vaccines: Priority activities to enable product development, licensure, and global access. *Vaccine* **39**, 4266-4277 (2021). https://doi.org:10.1016/j.vaccine.2021.04.018

51 Sheikh, A. *et al.* CEACAMs serve as toxin-stimulated receptors for enterotoxigenic Escherichia coli. *Proc Natl Acad Sci U S A* **117**, 29055-29062 (2020). https://doi.org:10.1073/pnas.2012480117

52 Sheikh, A. *et al.* Enterotoxigenic Escherichia coli degrades the host MUC2 mucin barrier to facilitate critical pathogen-enterocyte interactions in human small intestine. *Infect Immun*, IAI0057221 (2021). https://doi.org:10.1128/IAI.00572-21

53 Harris, J. B. Cholera: Immunity and Prospects in Vaccine Development. *J Infect Dis* **218**, S141-S146 (2018). https://doi.org:10.1093/infdis/jiy414

54 Pipaliya, N. *et al.* Spectrum of chronic small bowel diarrhea with malabsorption in Indian subcontinent: is the trend really changing? *Intest Res* **14**, 75-82 (2016). https://doi.org:10.5217/ir.2016.14.1.75

55 Ghoshal, U. C., Srivastava, D., Verma, A. & Ghoshal, U. Tropical sprue in 2014: the new face of an old disease. *Curr Gastroenterol Rep* **16**, 391 (2014). https://doi.org:10.1007/s11894-014-0391-3

56 Dutta, A. K., Balekuduru, A. & Chacko, A. Spectrum of malabsorption in India--tropical sprue is still the leader. *J Assoc Physicians India* **59**, 420-422 (2011).

57 Klipstein, F. A. & Falaiye, J. M. Tropical sprue in expatriates from the tropics living in the continental United States. *Medicine (Baltimore)* **48**, 475-491 (1969).

58 Klipstein, F. A. Tropical sprue in travelers and expatriates living abroad. *Gastroenterology* **80**, 590-600 (1981).

59 Kelly, P. *et al.* Gene expression profiles compared in environmental and malnutrition enteropathy in Zambian children and adults. *EBioMedicine* **70**, 103509 (2021). https://doi.org:10.1016/j.ebiom.2021.103509

60 Zyambo, K. *et al.* Reduced Fractional Absorption of Zinc in Children With Environmental Enteropathy in Zambia. *J Pediatr Gastroenterol Nutr* **74**, 277-283 (2022). https://doi.org:10.1097/MPG.0000000000003292

61 Long, J. M. *et al.* Zinc Absorption from Micronutrient Powders Is Low in Bangladeshi Toddlers at Risk of Environmental Enteric Dysfunction and May Increase Dietary Zinc Requirements. *J Nutr* **149**, 98-105 (2019). https://doi.org:10.1093/jn/nxy245

62 Lindenmayer, G. W., Stoltzfus, R. J. & Prendergast, A. J. Interactions between zinc deficiency and environmental enteropathy in developing countries. *Adv Nutr* **5**, 1-6 (2014). https://doi.org:10.3945/an.113.004838

63 Roy, S. K. *et al.* Impact of zinc supplementation on intestinal permeability in Bangladeshi children with acute diarrhoea and persistent diarrhoea syndrome. *J Pediatr Gastroenterol Nutr* **15**, 289-296 (1992). https://doi.org:10.1097/00005176-199210000-00010

64 Dhingra, U. *et al.* Lower-Dose Zinc for Childhood Diarrhea - A Randomized, Multicenter Trial. *N Engl J Med* **383**, 1231-1241 (2020). https://doi.org:10.1056/NEJMoa1915905

65 Kuhlmann, F. M. *et al.* Conservation and global distribution of non-canonical antigens in Enterotoxigenic Escherichia coli. *PLoS Negl Trop Dis* **13**, e0007825 (2019). https://doi.org:10.1371/journal.pntd.0007825

66 Zhang, X. *et al.* Genome-wide analysis of cAMP-response element binding protein occupancy, phosphorylation, and target gene activation in human tissues. *Proc Natl Acad Sci U S A* **102**, 4459-4464 (2005). https://doi.org:10.1073/pnas.0501076102

67 Mayr, B. & Montminy, M. Transcriptional regulation by the phosphorylation-dependent factor CREB. *Nat Rev Mol Cell Biol* **2**, 599-609 (2001).

68 Delghandi, M. P., Johannessen, M. & Moens, U. The cAMP signalling pathway activates CREB through PKA, p38 and MSK1 in NIH 3T3 cells. *Cell Signal* **17**, 1343-1351 (2005). https://doi.org:10.1016/j.cellsig.2005.02.003

69 Rohlff, C., Ahmad, S., Borellini, F., Lei, J. & Glazer, R. I. Modulation of transcription factor Sp1 by cAMP-dependent protein kinase. *J Biol Chem* **272**, 21137-21141 (1997). https://doi.org:10.1074/jbc.272.34.21137

70 Viollet, B., Kahn, A. & Raymondjean, M. Protein kinase A-dependent phosphorylation modulates DNA-binding activity of hepatocyte nuclear factor 4. *Molecular and cellular biology* **17**, 4208-4219 (1997). https://doi.org:10.1128/MCB.17.8.4208

71 Chen, L. *et al.* A reinforcing HNF4-SMAD4 feed-forward module stabilizes enterocyte identity. *Nat Genet* **51**, 777-785 (2019). https://doi.org:10.1038/s41588-019-0384-0

72 de Rooij, J. *et al.* Epac is a Rap1 guanine-nucleotide-exchange factor directly activated by cyclic AMP. *Nature* **396**, 474-477 (1998). https://doi.org:10.1038/24884

73 Bos, J. L., de Rooij, J. & Reedquist, K. A. Rap1 signalling: adhering to new models. *Nat Rev Mol Cell Biol* **2**, 369-377 (2001). https://doi.org:10.1038/35073073

74 Frische, E. W. & Zwartkruis, F. J. Rap1, a mercenary among the Ras-like GTPases. *Dev Biol* **340**, 1-9 (2010). https://doi.org:10.1016/j.ydbio.2009.12.043

75 Ogryzko, V. V., Schiltz, R. L., Russanova, V., Howard, B. H. & Nakatani, Y. The transcriptional coactivators p300 and CBP are histone acetyltransferases. *Cell* **87**, 953-959 (1996). https://doi.org:10.1016/s0092-8674(00)82001-2

76 Pattabiraman, D. R. *et al.* Activation of PKA leads to mesenchymal-to-epithelial transition and loss of tumor-initiating ability. *Science* **351**, aad3680 (2016). https://doi.org:10.1126/science.aad3680

77 Anders, S. & Huber, W. Differential expression analysis for sequence count data. *Genome Biol* **11**, R106 (2010). https://doi.org:10.1186/gb-2010-11-10-r106

78 Benjamini, Y. & Hochberg, Y. Controlling the False Discovery Rate: A Practical and Powerful Approach to Multiple Testing. *Journal of the Royal Statistical Society. Series B (Methodological)* **57**, 289-300 (1995). https://doi.org:10.2307/2346101

79 Kanehisa, M., Furumichi, M., Sato, Y., Ishiguro-Watanabe, M. & Tanabe, M. KEGG: integrating viruses and cellular organisms. *Nucleic Acids Res* **49**, D545-D551 (2021). https://doi.org:10.1093/nar/gkaa970

80 Gene Ontology, C. The Gene Ontology resource: enriching a GOld mine. *Nucleic Acids Res* **49**, D325-D334 (2021). https://doi.org:10.1093/nar/gkaa1113

81 Delannoy-Bruno, O. *et al.* Evaluating microbiome-directed fibre snacks in gnotobiotic mice and humans. *Nature* **595**, 91-95 (2021). https://doi.org:10.1038/s41586-021-03671-4

82 Sabui, S. *et al.* Hypoxia inhibits colonic uptake of the microbiota-generated forms of vitamin B1 via HIF-1alpha-mediated transcriptional regulation of their transporters. *J Biol Chem* **298**, 101562 (2022). https://doi.org:10.1016/j.jbc.2022.101562

83 Zawel, L. *et al.* Human Smad3 and Smad4 are sequence-specific transcription activators. *Mol Cell* **1**, 611-617 (1998). https://doi.org:10.1016/s1097-2765(00)80061-1

84 Anandam, K. Y., Srinivasan, P., Yasujima, T., Al-Juburi, S. & Said, H. M. Proinflammatory cytokines inhibit thiamin uptake by human and mouse pancreatic acinar cells: involvement of transcriptional mechanism(s). *American journal of physiology. Gastrointestinal and liver physiology* **320**, G108-G116 (2021). https://doi.org:10.1152/ajpgi.00361.2020

85 Howe, K. L. *et al.* Ensembl 2021. *Nucleic Acids Res* **49**, D884-D891 (2021). https://doi.org:10.1093/nar/gkaa942

86 Matys, V. *et al.* TRANSFAC and its module TRANSCompel: transcriptional gene regulation in eukaryotes. *Nucleic Acids Res* **34**, D108-110 (2006). https://doi.org:10.1093/nar/gkj143

87 Wang, J., Vasaikar, S., Shi, Z., Greer, M. & Zhang, B. WebGestalt 2017: a more comprehensive, powerful, flexible and interactive gene set enrichment analysis toolkit. *Nucleic Acids Res* **45**, W130-W137 (2017). https://doi.org:10.1093/nar/gkx356

88 Zhu, Y. *et al.* Molecular Determinants of Enterotoxigenic Escherichia coli Heat-Stable Toxin Secretion and Delivery. *Infect Immun* **86** (2018). https://doi.org:10.1128/IAI.00526-18

89 Sack, D. A., Huda, S., Neogi, P. K., Daniel, R. R. & Spira, W. M. Microtiter ganglioside enzyme-linked immunosorbent assay for vibrio and Escherichia coli heat-labile enterotoxins and antitoxin. *J Clin Microbiol* **11**, 35-40 (1980).

90 Tsang, V. C., Wilson, B. C. & Maddison, S. E. Kinetic studies of a quantitative single-tube enzyme-linked immunosorbent assay. *Clinical chemistry* **26**, 1255-1260 (1980).

91 Roy, K., Hamilton, D. J., Munson, G. P. & Fleckenstein, J. M. Outer Membrane Vesicles Induce Immune Responses to Virulence Proteins and Protect against Colonization by Enterotoxigenic Escherichia coli. *Clin Vaccine Immunol* **18**, 1803-1808 (2011). https://doi.org:10.1128/CVI.05217-11

92 Sixma, T. K. *et al.* Refined structure of Escherichia coli heat-labile enterotoxin, a close relative of cholera toxin. *J Mol Biol* **230**, 890-918 (1993). https://doi.org:10.1006/jmbi.1993.1209

93 Love, M. I., Huber, W. & Anders, S. Moderated estimation of fold change and dispersion for RNA-seq data with DESeq2. *Genome Biol* **15**, 550 (2014). https://doi.org:10.1186/s13059-014-0550-8

94 Evans, D. J., Jr. & Evans, D. G. Three characteristics associated with enterotoxigenic Escherichia coli isolated from man. *Infect Immun* **8**, 322-328 (1973).

95 Dorsey, F. C., Fischer, J. F. & Fleckenstein, J. M. Directed delivery of heat-labile enterotoxin by enterotoxigenic Escherichia coli. *Cell Microbiol* **8**, 1516-1527 (2006). https://doi.org:10.1111/j.1462-5822.2006.00736.x

Acknowledgements

JMF was supported by funding from the National Institute of Allergy and Infectious Diseases (NIAID) of the National Institutes of Health (NIH) R01 AI126887, R01 AI089894, U01 AI095473; and the Department of Veterans Affairs (5I01BX001469-05). Research conducted by AS was also supported by National Institute of Allergy and Infectious Diseases of the National Institutes of Health under Award Number T32AI007172. We thank the Genome Technology Access Center in the Department of Genetics at Washington University School of Medicine for help with genomic analysis. The Center is partially supported by NCI Cancer Center Support Grant #P30 CA91842 to the Siteman Cancer Center and by ICTS/CTSA Grant# UL1TR002345 from the National Center for Research Resources (NCRR), a component of the National Institutes of Health (NIH), and NIH Roadmap for Medical Research. HMS was supported by funding from the Department of Veterans Affairs (I01BX001142) and the National Institutes of Health (DK5606 and AA018071). HMS is recipient of a Senior Research Career Scientist award # IK6BX006189.

The content is solely the responsibility of the authors and does not necessarily represent the official views of the National Institutes of Health, or the Department of Veterans Affairs.

Interests Declaration

R.D.H. and C.S. may receive royalty income based on the CompBio technology developed by R.D.H. and licensed by Washington University to PercayAI.